Contents lists available at ScienceDirect

Arabian Journal of Chemistry

journal homepage: www.ksu.edu.sa

Original article

Formulation, characterization and evaluation of anti-breast cancer activity of 2-carene nanoemulsion; *in silico*, *in vitro* and *in vivo* study

Iffat Nayila [a,b,*], Sumaira Sharif [b], Madeeha Shahzad Lodhi [b], Riaz Ullah [c], Amal Alotaibi [d], Tahir Maqbool [b], Saima Hameed [e]

[a] Department of Pharmacy, The University of Lahore Sargodha Campus. Sargodha, Pakistan
[b] Institute of Molecular Biology and Biotechnology, The University of Lahore. Lahore, Pakistan
[c] Medicinal Aromatic and Poisonous Plants Research Center, College of Pharmacy, King Saud University, Riyadh (RUH) 11421, Saudi Arabia
[d] Department of Basic Science, College of Medicine, Princess Nourah bint Abdulrahman University, P.O. Box 84428, Riyadh 11671, Saudi Arabia
[e] Institute for Advanced Study, Shenzhen University, Shenzhen 518060, PR China

ARTICLE INFO

Keywords:
Breast cancer
Phytocompounds
Nanoemulsion
Terpene
Apoptosis
Essential oil
Cytotoxicity

ABSTRACT

Natural phytocompounds extensively used in several therapeutic regimes, biomedical and pharmaceutical applications and their nanoparticles have become extremely essential in field of nanotechnology to treat various types of cancer. The main objective of this study demonstrates the antitumor activities of pure terpene compound 2-carene and its nanoemulsion against *in vitro* and *in vivo* breast cancer model. *In silico* and molecular dynamic simulation study was performed against breast cancer receptors to evaluate anticancer activity of 2-carene. Nanoemulsions were prepared by isolating monoterpenoid compound from *Catharanthus roseus* essential oil and anti-cancer effects of 2-carene mediated nanoemulsion were evaluated. Gas chromatography-mass spectrometry analysis explicated 2-carene was the active terpene compound and nuclear magnetic resonance spectroscopy was performed to confirm structural identification of this compound. Nanoemulsion was characterized by characteristic techniques of scanning electron microscopy, Fourier transform infrared spectroscopy, size determination and dynamic light scattering. Cytotoxicity, antioxidant activity, apoptosis and histopathological examination were used to identify bioactive qualities of prepared nanoemulsion formulation. Effective cytotoxicity of nanoemulsion was observed 54.31% against MDA-MB-231 cancer cell lines. Tumor features and apoptotic activity was also assessed and the results of study strongly revealed that bio-synthesized nanoemulsion show significant apoptotic and anti-tumor potential against DMBA induced breast cancer. The antioxidant enzymes and serum inflammatory markers were significantly improved by nanoemulsion treatment in cancer induced rat model. In histopathological evaluation, the nanoemulsion formulations markedly show signs of improvement in cancer induced tissues. Results demonstrated that 2-carene and its synthesized nanoemulsion exhibit remarkable anticancer potential against DMBA induced cancer.

1. Introduction

Breast cancer is one of the main causes of death from cancer malignancies among women. Innovative target therapies possess the capability to significantly enhance the overall survival rates of breast cancer patients. Accurate detection of breast cancer is enormously important for diagnosis and treatment (Johnson et al. 2013). A new approach to addressing the severity of breast cancer was used for targeted medication delivery systems and some unique methodologies for anti-cancer treatment (Gurunathan et al. 2013). Regular monitoring and identification of diagnostic parameters have provided a thought provoking landscape for patients. A variety of biochemistry and molecular biomarkers, such as enzymes, serum biomarkers, antioxidants levels and gene expression profiles are convenient for the accurate diagnosis and

Abbreviations: ADMET, Adsorption, metabolism, distribution, excretion, and toxicity; EO, Essential oil; GC/MS, Gas chromatography–mass spectrometry; HER2, Human epidermal growth factor receptor 2; IL-1, Interleukin 1; IL-6, Interleukin-6; MD simulations, Molecular Dynamics simulations; MDA-MB-231, Epithelial, human breast cancer cell line; MTT, Dimethylthiazol Diphenyltetrazolium; NF-kB, Nuclear factor kappa B; NPs, Nanoparticles; RMSD, Root mean square deviation; RMSF, Root mean square fluctuations; SOD, Superoxide dismutase; TNF-α, Tumor necrosis factor-α.

* Corresponding author at: Deparment of Pharmacy, The University of Lahore Sargodha Campus, Sargodha, Pakistan.
E-mail address: iffat.nayila@uipt.uol.edu.pk (I. Nayila).

https://doi.org/10.1016/j.arabjc.2024.105937
Received 20 March 2024; Accepted 23 July 2024
Available online 25 July 2024

treatment of breast cancer and metastatic disease (Kaplan, Malmgren, and Atwood 2017). Numerous anti-inflammatory plants natural components have been found and described in traditional medicinal remedies. Studies to this extent have shown that phytochemicals administered as whole or isolated molecules have several advantages over synthetic medications in the therapy of life threatening malignancies and immune dysregulation diseases (Liyanage et al. 2019). A thorough comprehension of their method of action will give justification for their use in modern therapeutic clinical strategies when combined with traditional anticancer medications. These results show a correlation between the antioxidant capabilities and immune stimulating effects of phytochemicals and nanoformulations synthesized by natural plant compounds (Samec et al. 2020).

Nanoparticles have much significance in a number of disciplines because of their astonishing potentials, such as structural efficacy, size stability, sub-micron size and improved targeting systems (Boisseau and Loubaton 2011). To enhance the prospective use of natural compounds, nanotechnology has been used to develop novel formulations to target malignant cells (Verma, Fatima, and Ansari 2022). They can be used to deliver anticancer medications to particular sites by targeting some high affinity receptors that are overexpressed in these tumor cells (Malik et al. 2022). Entrapment of anticancer medications in nanoparticles can control the cellular distribution and bioavailability profiles of these drugs. The targeted distribution of biosynthesized molecules to tumor cells is an additional advantage of phytocompound loaded nanoparticles. A significant problem in chemotherapy is that some chemotherapy agents have an intriguing ability to reverse drug reactions (Brigger, Dubernet, and Couvreur 2012). It has been observed that nanoformulations can enhance medication delivery, bioavailability and minimize chemotherapy related unwanted effects (Gavas, Quazi, and Karpiński 2021). Nanoformulations of natural substances can increase the efficacy and bioavailability of natural compounds and even regulate the drug delivery mechanism of phytochemicals to targeted areas (Verma, Fatima, and Ansari 2022).

Catharanthus roseus is a viable treatment candidate that may slow the spread of breast cancer by preventing the disease from spreading (Eltayeb et al. 2016). In addition to having the highest concentration of phytocompounds with significant antioxidant capacity, a study on *C. roseus* revealed that it had potent anti-proliferative activity against a variety of cancer cell lines, making it a promising source for the investigation of pure active compounds to be used in cancer medicines (Pham et al. 2019). *C. roseus* extract has shown a strong suppressive effect to invade in tumor cells, as well as reducing the activity of metastatic cells (Eltayeb et al. 2016). The toxicity assessment against human red blood cells advised that essential oil (EO) and phytocompounds based nanoparticles possess better cytotoxicity. Altogether, it was suggested that NPs are valued biomaterials owing to their capability to fight against cancer (Rajivgandhi et al. 2020). Phytocompound terpenes have been demonstrated to possess cytotoxic, antimicrobial, and anticancer properties (Greay and Hammer 2015). As terpenes and terpenoids targeted major cancer signaling pathways and were used as complementing chemotherapeutic treatments by minimizing some drug related unwanted effects such as bleeding, irregularities in complete blood count profile, immunocompromised reactions and cytotoxicity effects against healthy cells (Tomko et al. 2020). Terpenes are normally found in 2–5 % concentrations in essential oils but they can be present at considerably higher amounts in a variety of different products such as herbal and medicinal plants. However knowledge about many terpenes and their potential therapeutic medicinal effects is still unknown (Booth and Bohlmann 2019).

Thus, in the present study the monoterpenoid 2-carene, which was isolated from *Catharanthus roseus* essential oil, was evaluated using computational docking study against few BC targets and then biosynthesized nanoemulsion of 2-carene was formulated, characterized and its potential against breast cancer cell lines and DMBA induced breast cancer rat model was examined.

2. Materials and methods

2.1. Essential oil extraction

Fresh plants of *Catharanthus roseus* that were gathered from nearby local nurseries. At Agriculture University Faisalabad, a voucher specimen was deposited (181–1-23). After being air-dried at 25 to 28 °C, fresh plant material was ground into a powder. A laboratory scale Clevenger-style hydro-distillation system was used for hydrodistillation of essential oil conducted at 100 °C for four to six hours. 2.5 L of water was added as solvent to dried plant powder weighing 150 g. After the dried plant was hydro-distilled, the yield of essential oil obtained was calculated. For GC–MS analysis and phytocompound isolation, the extracted essential oil was stored in a sealed glass vial at 4 °C. (Conde-Hernández et al. 2017).

2.2. GC/MS analysis

A gas chromatography approach combined with a mass spectrophotometer was used to accomplish the GC/MS analysis of EO. Helium was used as the carrier gas, and 1:100 split ratio was used together with a direct injection of the essential oil (0.1 µL) (Furuhashi and Okuda 2017). The oven was preheated to 50 °C for one minute, and then at 25 °C/min temperature gradient. The temperature was maintained constant for 20 min after it hit 160 °C. After that, the oven temperature was raised by 5.0 °C every minute for 15 min, to reach 250 °C. One milliliter per minute of helium was employed as the carrier gas. The temperature of the injector and transfer line were both set to 250 °C. Setting the electron energy to 70 eV allowed the mass spectrometer to function in the electron impact mode. The conventional procedure of identifying volatiles involved comparing mass spectra and Kováts Indices using the National Institute of Standard and Technology (NIST) library's database (Spyridopoulou et al. 2019).

2.3. Isolation of terpene

Column chromatography was used as a subsequent purification step to isolate the compound from *C. roseus* essential oil. Despite using a mobile phase of solvents consisting of methanol and ethyl acetate (7.6:2.4) in column chromatography, E. Merck's silica gel 60 (mesh size 70–230) was utilized. To conduct column chromatography, the *C. roseus* essential oil was diluted in solvents and triturated using silica. A glass column was filled with a silica gel and solvent slurry. After a few hours, the sample was put to the top of the packed column using the wet-packing technique. When the column's valve was opened, 10 to 20 ml of solvent that was released and were collected in test tubes. Samples separated from column fractions were examined using thin layer chromatography (TLC) plates in acetone: ethyl acetate (4:2, v/v) solvent systems to find the retention factor (Rf) of components that appeared as spots. Following solvent separation, the proportion of separated components was computed (Ngo and Chua 2019).

2.4. Characterization of terpene

The ^{1}H NMR and ^{13}C NMR spectra were measured at 500 and 125 MHz, respectively, using a JEOL JNM-ECA 500 Spectrometer for NMR spectroscopy. The methodology employed was, with minor adjustments, that of Kim et al (Kim et al. 2023). The sample was put into a different, 2-milliliter microtube and added 0.5 ml of CD_3OD and 0.5 ml of KH_2PO_4 buffer (pH 6.0) in D_2O. To generate a clear supernatant, the mixture was centrifuged (Centrifuge MPW-260, Instruments, Poland) at 13,000 rpm for 10 about minutes after being vortexed (Vortex Mixer, Thermo Fisher Scientific, USA) for 1 min and ultrasonicated for 20 min. A volume of 0.8 ml supernatant was transferred to an NMR tube promptly. Sample was subjected to ^{1}H NMR using a preset setting after about 0.8 mL of the supernatant was transferred NMR tube. A 500 MHz NMR Spectrometer

(JEOL ECZR, JEOL Ltd., Tokyo, Japan) was used to perform the ^{1}H NMR experiments (Rohman et al. 2020). Based on available database of NMR absorptions and proposed structure provided by the NIST library, https://www.nist.gov/nist-research-library each ^{1}H NMR and ^{13}C NMR observed were determined (Efdi et al. 2010).

2.5. *In silico prediction and computational analysis*

2.5.1. *Docking tools and protein selection*

For computational *in silico* study, software used are Python, the Desmond simulation package of Schrodinger and Discovery Studio 4.0, ChemDraw 3D Pro 12.04v, Auto dock tools in Auto-dock 4.6 program and PubChem database. The three-dimensional protein structures of the human estrogen receptor, human progesterone receptor and HER2 receptor (PDB id: 2iok, 1e3k and 3 pp0 respectively) were downloaded with the protein databank (https://www.rcsb.org/pdb/ home/home.do) (Fig. 1). In order to advance docking, the structure was arranged and refined, every receptor's binding site was examined, and protein files were created using the AutoDock4 application and saved in PDBQT format.

3D structure of 2-carene was attained from open-source PubChem (https://pubchem.ncbi.nlm.nih.gov/) and transformed into PDB files using Open Babel (Boyles, Deane, and Morris 2020).

2.5.2. *ADME analysis and toxicity screening*

ADME analysis includes predictions about the absorption, transportation, metabolism, and excretion of a drug into different human tissues for predicting pharmacokinetic features (Gleeson et al. 2011). After virtual screening, the 2-carene was next submitted to ADME study utilizing ADMET 2.0 (https://admetmesh.scbdd.com) server tool (Daina, Michielin, and Zoete 2017).

In the context of pharmaceutical research, "*in-silico* toxicity-based screening" refers to the use of computer based methods to forecast potentially hazardous side effects of a therapeutic molecule. These methods offer information about the toxicity of compounds that have been found (Fernando et al. 2019) Using *in-silico* approaches, one can forecast the likely side effects and potentially harmful consequences on certain organ systems of a pharmaceutical candidate. This can lower the price of animal testing while also hastening the medication development process. Following ADME and drug likeliness tests, *in-silico* techniques were used to evaluate the toxicity of 2-carene, and the ADMET 2.0 server was utilized to further explore the toxicity of the compound https://admetmesh.scbdd.com) (Xiong et al. 2021).

2.5.3. *Molecular dynamics simulation*

Biological molecular dynamics are investigated in a simulated environment by computational MD simulation techniques. The method integrates the equations of motion to show the interactions between atoms or molecules (Sousa da Silva and Vranken 2012). MD simulations can be used to compute the binding affinities of pharmaceuticals, identify possible binding sites, and examine how drugs interact with the desired protein targets (Shaldam et al. 2021) and (Duran et al. 2021) Desmond module (Schrödinger Release 2020–4) package was used to run simulation of 2-carene top docked complex.

2.6. *Nanoemulsion formulation*

2-carene mediated nanoemulsion was prepared following (Periasamy, Athinarayanan, and Alshatwi 2016) with adjustments. Nanoemulsion was formulated using Tween 80 (12.2 % v/v) and Tween 20 (8 % v/v) to formulate nano-sized droplets and to preserve particle's stability. A homogeneous aqueous phase was produced by swirling mixture of double-distilled water (69.8 % v/v) and surfactant for 50 min and then 2-carene (10 % v/v) was added dropwise and stirred gently for 20 min at 8000 RPM. It was thought that sonication and the self-emulsifying process could work together to improve the stability of the nanoemulsion. As it was high energy emulsification process so the procedure was conducted in an ice bath and the emulsion was sonicated for ten minutes using a 20 kHz sonicator (Ultrasonic Processor, GEX 750, USA) with power output of 750 Watt (Navaei Shoorvarzi et al. 2020). After ensuring that all of the solvent had been removed from the emulsion, it was centrifuged at 4000 rpm for four hours at room temperature. The nanoemulsion was subsequently employed for additional characterization after being filtered using a membrane syringe filter to remove contaminants and to separate extra amount of surfactant concentration. The entire process of creating the 2-carene-mediated nanoemulsion was carried out in the dark and at a regulated temperature because terpene chemicals are volatile by nature and sensitive to light.

2.6.1. *Entrapment efficacy of nanoemulsion*

The spectro-photometric measurement of drug loading and entrapment efficiency of 2-carene nanoemulsion was conducted using a spectrophotometer (Lambda Bio 20 UV/VIS) (Perkin Elmer, Waltham, MA). Nanoemulsion sample was centrifuged at 13600 rpm for 20 min after a known amount of nanoemulsion (10 mg) was used. The solution's absorbance was calculated at 273 nm. Using the standard curve that was created between the different sample amounts and absorbance (optical density), the amount of 2-carene was determined. Using the following formula, the percentages for drug-loading and entrapment efficiency (% EE) were determined. Three duplicates of each measurement were made (Srivastava et al. 2013).

Entrapment efficacy (%) = Actual drug content in nanoparticles / Total amount of drug used x 100.

2.6.2. *Characterization of nanoemulsion*

Zeta sizer, PDI, and dynamic light scattering analysis were used to

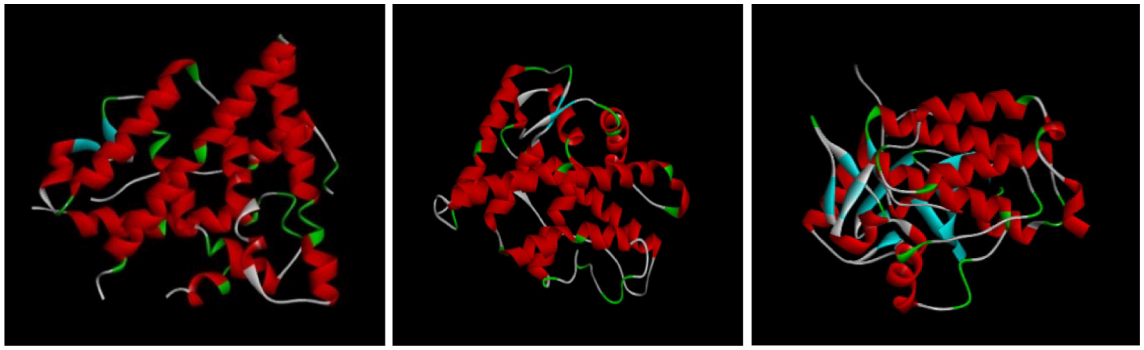

Fig. 1. Breast cancer receptors used for *In silico* study.

examine synthesized nanoemulsion. These measurements demonstrate a nano-emulsion's stability and homogeneity. Malvern Zeta Sizer was employed to measure the particle size of the nano-emulsion, while an ultra violet/visible (UV) spectrophotometer and Fourier transformed infra-red (FTIR) parametric analysis were utilized to assess the homogeneity of oil droplets in nanoparticles (Abadi et al. 2021).

2.6.3. Particle size determination

With a Zetasizer Nano-ZS (Malvern Instruments, Malvern, UK) and 5 mWatt He-Ne laser operating at 633 nm wavelength, particle size as well as zeta potential of the nanoemulsion were ascertained using a dynamic light scattering technique. After the nanoemulsions were combined with 1 mg/mL of phosphate buffer (pH 7.2–7.4), the average of 20 and 30 trials in triplicate were used to calculate the nanoemulsions' size and zeta potential. The data analysis was done automatically, and the Smoluchowski approximation was used to determine the average values based on the electrophoretic mobility (Bhattacharjee 2016).

2.6.4. pH and viscosity determination

1.5 ml of the nano-emulsion and 9.0 ml of distilled water were added to a test tube and homogenized. A digital pH meter (Mi,151 martini Instruments) was used to determine the pH value by inserting the electrode directly into the sample. The nano-emulsion was deemed stable and was kept in three distinct temperatures: 4 ± 3 °C, 25 ± 4 °C (room temperature), and 40 ± 4 °C. These were the settings under which the samples were kept for 40 days. A glass tube was filled with prepared nanoemulsion up to three milliliters, and during the storage time, the transition from a steady state to aggregation and cohesiveness was examined. A rotary myr VR 3000 digital viscometer was used to measure the viscosity of produced nanoemulsions at 25 °C at 200 rpm without any dilution (Agrawal and Mishra 2017)

2.6.5. UV/visible and FT-IR spectroscopy

The wavelength of light that a substance absorbs determines its chemical composition. There is a connection between the absorption of visible and ultraviolet (UV) light and the stimulation of electrons (atoms and molecules) to higher energy levels. The absorbance mode of a UV–Visible spectrophotometer (Jasco SLM-468, Japan) was utilized to investigate the turbidity of the nanoemulsion at a wavelength of up to 1000 nm (Uncu, Ozen, and Tokatli 2019).

Fourier transform infrared spectroscopy of terpene mediated nanoemulsion were obtained using the conformist KBR disk/pallet method (SHIMADZU, Model 8400S, Tokyo, Japan). Following a 1:150 ratio of sample and KBr, the mixture was compressed using a Jasco micro hydraulic compactor (Jasco, Japan). To put it briefly, the samples were ground and then crushed into a pellet using anhydrous KBr. Using the 400–4000 cm^{-1} wavelength range, the FT–IR spectra were produced (Bhattacharya 2020).

2.6.6. Scanning electron microscopy and edx spectroscopy

The morphology of the terpene nanoemulsion was examined using scanning electron microscope (SEM) (Hitachi High Technology, SU9000). The SEM apparatus can resolve images at 0.4 nm at 30 kV with greater stability. A tiny quantity of dispersion was spread over a coverslip and dried at room temperature in order to identify the morphology of the first 50 µl nanoemulsion, which had been diluted with 1 mL of distilled water. A glass sputter coater operating at a higher vacuum state was used to coat the dried film, and a SEM high-pressure method was used to scan the nanoemulsion sample at a working distance of x5000 magnification (Bhattacharya 2020). Energy dispersive x-ray (EDX) analysis is a technique used in elemental analysis. Oxygen, zinc, silver and other fundamental elements are confirmed to exist using this technique. With the use of SEM, the sample's EDX analysis was found. The graphs display the signals from the instrument, and samples were made on holy carbon grids (Tüzün, Hohmann, and Kivcak 2018).

2.7. DPPH antioxidant activity

The antioxidant potential of natural phytocompounds and nanoformulations was assessed using the DPPH antioxidant test. 5 mL of methanolic DPPH (0.2 mmol/L) solution was mixed with 3 mL of a selected concentration of 2-carene and nanoemulsion at different concentrations (0.25, 0.5, and 1 mg/ml), using ascorbic acid as a standard reference. The content was incubated at room temperature in the dark for thirty minutes. Using a UV wavelength of 516 nm, the sample's absorption activity was measured in triplicate. The inhibitory action was ascertained as the percentage of DPPH decreased relative to the control. To determine the inhibitory action, the percentage of DPPH that decreased relative to the control was utilized (Valko et al. 2007).

2.8. Cytotoxicity analysis (MTT assay)

Anti-proliferative activity and cell viability of 2-carene and 2-carene induced nanoemulsion were assessed using the MTT (3-(4,5-dimethylthiazol-2-yl)-2,5-diphenyltetrazolium bromide) test,. The University of Lahore's Institute of Molecular Biology and Biotechnology department provided the MDA-MB-231 breast cell lines and the HMEpC healthy epithelial cells. A density of 6 x 103 cancer cells were injected into microtiter plate wells using 100 µL of cell media per well. The plate is then incubated in a CO_2 incubator for an extra night to promote cell adherence. Separate additions of test complexes (2-carene and varying nanoemulsion concentrations) were made to every well that contained cells. The plates were housed in an incubator at 37 °C for 72 h. After four hours, each well was re-incubated with 20 µl of MTT reagent. The plates were then scanned using a traditional ELISA microplate reader at 570 and 620 nm wavelengths (Luis et al. 2019).

2.8.1. Crystal violet assay

Using the crystal violet staining method and an established protocol, the maximal cytotoxicity concentration of 2-carene and biosynthesized nanoemulsion as well as the viability of MDA-MB-231 cell lines and HMEpC cells were ascertained (Maqbool et al. 2019). After the media from each experimental group was removed, the 96-well plate utilized for this procedure was cleaned with PBS. The wells were cleaned, and then 0.1 % crystal violet dye and 2 % ethanol were added. It was incubated for fifteen minutes at room temperature. In order to prevent cells from rising to the surface, wells were thoroughly cleaned and dye was disposed of. Next, the dye was solubilized by filling each well with 200 µl of 1 % SDS, and the absorbance at 540 nm was recorded on a microtiter plate.

2.9. Cancer induced experimental study

Weighting between 150–170 g, adult female SD rats were attained from the Institute of Molecular Biology and Biotechnology, University of Lahore's research animal facility. Institutional animal ethics strictly followed the guidelines for monitoring and controlling experimental animals. A climate-controlled chamber with a 12-hour light/dark cycle, 50 % humidity, and a 24–27 °C temperature range was employed to house the rats. After a certain amount of days for acclimation, rats were divided into six groups having seven rats into each group. To promote breast cancer in rats, 25 mg/kg DMBA (7, 12-dimethylbenz[a]anthracene), (product number D807576-100 mg MACKLIN, China.) was administered (Arroyo-Acevedo et al. 2015). Rats in the control group were not exposed to DMBA or treated with nanoemulsion, rats in the positive control group were given only 50 mg/kg of nano-emulsion, and rats in the DMBA group were given 25 mg/kg of DMBA without being treated with 2-carene or nanoemulsion. Rats in 2-carene treated group were given 25 mg/kg of cancer drug and 25 mg/kg of 2-carene terpene compound, rats in the nano-emulsion treatment group were given 50 mg/kg of nanoemulsion after cancer induction and rats in the EO group were exposed to 25 mg/kg of DMBA drug and then 25 mg/kg of EO.

Following four to five weeks of intraperitoneal injection of a single dosage of DMBA, cancer was generated and tumor palpation was noted in animals administered with DMBA. Subsequently the tumor was induced, EO, 2-carene, and synthesized nanoemulsion therapies were given intra-gastrically for four weeks at predetermined times on different days. To take blood samples, a cardiac puncture was performed with a sterile needle. Following the separation of the blood sample into two fractions, the first was transferred to plain sample tubes, and the second, including complete blood samples, was transferred to EDTA sample collecting tubes. In order to extract serum, blood was spun at 3000 rpm to separate the serum from the plasma. Following centrifugation, serum samples were stored at −20 °C until their cytokine cancer and stress indicators were examined. To prevent cell hemolysis, the anticoagulant was able to mix with the blood samples in the EDTA vials by gently shaking them. Immediately upon the collection of blood samples, the hematological and biochemical tests were performed.

2.9.1. Extent of tumor volume and tumor ratio

After DMBA was administered to the rats in each experimental group, changes in the tumor growth rate in each group for four to five weeks before starting treatment with isolated terpene compound and nano emulsion were observed. Tumor size and animal weight were monitored on a regular basis. A Vernier caliper was used to measure the tumor size, tumor volume and growth rate. Rats with palpable tumors were examined, and the tumor volume was measured using the length and breadth diameters. The tumor growth ratio (V/V0) was computed by dividing the treated group's ultimate tumor size by the starting tumor growth (Talkington and Durrett 2015).

2.9.2. Apoptosis assay

Standard kits were utilized to measure the apoptotic activity of rat breast cancer samples in accordance with the manufacturer's recommendations. After staining apoptotic cells with Annexin VFITC/PI kit (Cat. No. E0457Ra), ELISA analysis was used to evaluate the outcomes. 50 µl of the standard solution was added to each well, and then 40 µl of the sample and 10 µl of the anti-ANX-5 antibody were added to the wells. Fill each well with 50 µl of substrate solution A and then 50 µl of substrate solution B. Wait ten minutes following the addition of the stop solution before using a microplate reader calibrated for 450 nm analysis to measure the optical density of each well (Lindemann et al. 2007).

2.9.3. Inflammatory marker analysis

Using ELISA kits and following the manufacturer's instructions, samples from each experimental group were examined for cytokines markers and interleukins, interleukin-1, interleukin −6, interleukin –23, and tumor necrotic factor-alpha. ELISA was used to quantify IL-1, IL-6, IL-23, and TNF-a utilizing Ready-SET-BT lab Kits (IL-1, E0107Ra; IL-23, E0125Ra; TNF-a, E0764Ra and IL-6, E0684). On each pre-coated plate, standard solutions, a designated antibody, control samples, and test samples were added. All procedures, including washing the plates and adding the antibodies, substrates, and stop solution, were carried out in accordance with the manufacturer's instructions (Jang et al. 2013).

2.9.4. Biochemical analysis

The levels of hematological indices, such as hemoglobin (Hb), lymphocytes, red blood cells (RBC), platelets, monocytes, and white blood cells (WBC), were measured using a hemato-analyzer (Abacus 380). Serum biochemistry was performed on every sample that was collected.

2.9.5. Oxidative stress markers

Antioxidant parameters were assessed from serum samples of 2-carene and nanoemulsion treated animals as indicators of oxidative stress using ELISA kits and standard protocols (Gyurászová et al. 2018).

The WST-1 formazan dye can be determined by spectrophotometric analysis at 450 nm. The total super oxide dismutase activity was measured using the SOD test kit (WST-Sigma Aldrich, Switzerland). The assay was completed in accordance with the manufacturer's protocol, and the absorbance was measured using a microplate reader after the plate had been incubated for 20 min at 37 °C (Weydert and Cullen 2010). Meanwhile the presence of catalase was ascertained using the Aebi (1974) method. 50 µL of 10 % homogenate should be added to a container along with 1.95 mL of pH 7.0 potassium phosphate buffer and 1 mL of 30 mM H2O2.(Aebi 1974). The absorbance was measured at 240 nm after 30 s and again after a 15-second delay (Hadwan 2018). Paglia and Valentine determined glutathione peroxidase activity. The reduction of hydrogen peroxide is catalyzed by GPx, which also oxidizes reduced glutathione to generate oxidized glutathione. The fall in absorbance at 340 nm, which can be quantified spectrophotometrically, is caused by NADPH oxidation (Duda et al. 2016). Sedlak and Lindsay (1968) reported that the GSH level was determined by centrifuging a 10 % tissue homogenate at 1000 rpm for five minutes after precipitating it with 50 % trichloroacetic acid. Next, 0.5 ml of the supernatant was combined with 2 ml of Tris EDTA buffer and mixed with 0.1 ml of 5,5-dithio-bis-(2-nitrobenzoic acid) (DTNB) solution. At 412 nm, the absorbance of the reaction mixture was measured (Rahmani et al. 2022).

2.9.6. Histopathological analysis of mammary tumor

At the conclusion of the study, specimens of breast tumors were removed from animals that had been slain. They were then preserved in buffered formalin, washed, and fixed for a full day at room temperature using 4 % paraformaldehyde. Cut the sample slices and paraffin-embedded sections of the fixed tissue (5 mm thick) were used. The slices were washed with tap water following a 10-minute staining process with hematoxylin. After sealing the slices with neutral glue, a digital photo camera was used to take pictures under an optical microscope (da Silva and Langoni 2001).

2.10. Statistical investigation

Every experiment's levels of examination were compared to those of the vehicle control group, nanoemulsion control group and the DMBA-induced group (which was not given any treatment). Versions 8.5. of the graph pad prism program and SPSS statistics software (SPSS Inc., USA) were used for the statistical analysis. ANOVA was applied to look for differences between each sample's means, and Dunnett analysis was accomplished. 0.05, 0.001, and 0.0001p value was employed to assess significant values.

3. Results

3.1. GC–MS analysis of essential oil

Phytocompounds present in essential oils act as secondary metabolites, which are intricate blends of volatile chemical compounds. The essential oil was extracted with 6.41 ± 0.21 % concentration, indicating that hydro distillation was used to extract a considerable amount of essential oil from *C. roseus*. (Supplementary figure S1). (Percent compositional data is also given in (Supplementary data table T1). The isolated chemical, 2-carene, was determined with RT (time taken for solute to pass through a chromatography column) 15.772. The compound's computed retention index (RI, which is retention time interpolated between neighboring n-alkanes) was 1171, while the RI reported in the literature is 1186. (This compound previously been reported to occur in *Fagonia longispina* (Ourzeddine et al. 2017).

3.2. FT-IR and NMR spectroscopy analysis

The GC–MS analysis showed retention time of 2-carene at 15.772 min and the molecular ion peak for this sample appeared at 136.2 amu. The prominent fragmentation pattern involved loss of methyl group and the FT-IR spectrum of 2-carene reflected absence of any prominent functional group. There was no indication of presence of hydroxyl or

amine functionality, carbonyl moiety was also not indicated from IR spectrum. However, the FTIR spectrum did indicate presence of C=C which appeared around 1446 cm^{-1}. Stretching corresponding to sp^3 hybridized C–C-H were also prominent this indicating the isolated compound to be a hydrocarbon with some degree of unsaturation (Supplementary figure S2).

NMR analysis of compound was obtained by proton (^1H) and Carbon (^{13}C) NMR to integrate selected compound. The ^1H NMR of compound indicated presence of 3 methyl groups; two methyl groups appeared at 1.06 δ (ppm) as a single of 6 proton integration and one methyl group appeared at 1.69 ppm. 2 protons appeared as a multiplet from 2.21 to 2.34 δ (ppm), 4 protons appeared as multiplet from 2.59 to 2.66 δ (ppm) while a single proton appeared as a doublet at 5.46 δ (ppm). The signal at 5.46 δ (ppm) indicated presence of a single olefinic proton. The ^{13}C NMR indicated presence of 6 aliphatic carbons and two olefinic carbons. The aliphatic carbons appeared at 21.2, 22.9, 24.0, 27.5, 31.6 and 34.6 δ (ppm) while the olefinic carbons appeared at 115.9 and 118.9 δ (ppm). From this spectroscopic, IR spectrum and spectrometric data, the isolated terpene compound was identified as 2-carene and NMR spectral data of proton assigned and carbon assigned was shown in Supplementary figure S3 and Supplementary figure S4.

3.3. Molecular docking study

Docking studies were conducted using the modeled 3D structures of ER, PR, and HER2 in order to better understand the interaction between 2-carene and breast cancer receptors. Clear observations of the hydrogen bonding molecules and free binding energy were made; the binding's negative least free energy value indicates a strong, advantageous link between the estrogen and HER2 receptor, with 2-carene in the most advantageous conformations. 2-carene showed better interaction with ER protein and showing hydrogen interaction with amino acid residues of ALA 351, TRP 383and GLU 353 and showed binding score of −6.3 kcal/mol. 2-carene compound when docked with progesterone receptor, showed *Van Der waals* interaction with amino acid residues of LEU 718 and THR 894 with binding score of −6.3 kcal/mol. Isolated compound 2-carene show *Van Der waals* interaction with amino acid residues SER 783, THR 798, ASP 863, LYS 753 and showed binding score of −6.6 kcal/mol with HER2 receptor. The results are displayed in Table 1. Ligand-protein visualization was shown in Figs. 2 and 3D interaction of 2-carene with BC targets displayed in Fig. 3. From binding affinity score, it was detected that 2-carene docked fine with HER2 protein with high docking value −6.6 kcal/mol and multiple hydrophobic interactions.

3.3.1. ADME analysis

The molecular structure of 2-carene was found to include seven number of atoms in the biggest ring. With a synthetic accessibility value of 3.659, the molecule was well regarded, and the ligand demonstrated significant gastrointestinal absorption and blood–brain barrier permeability. Lipinski's rule of five, gastrointestinal retention characteristics and PAINS,alert was widely used measure of drug-likeness to screen 2-carene. A medication that exhibited no PAINS signs, had substantial gastrointestinal retention, and satisfied Lipinski's rule of five was used for further testing. Table 2 presented the ADME parameters of the 2-carene. In the BOILED-Egg model, as shown in supplementary Figure S5, the white part represents the GI tract's passive absorption whereas the yellow region (yolk) indicates BBB penetration and findings demonstrated that 2-carene show substantial absorption and have high expected distribution volumes (VDss).

3.3.2. Toxicity screening analysis

By carrying out the ADME analysis, the toxicity profile of 2-carene was assessed. With the HER2 receptor acting as the anticancer target, 2-carene was utilized to assess the compound toxicity profile. Table 3 indicates that 2-carene exhibited mild irritating properties, it did not exhibit any signs of carcinogenesis, mutagenesis activity, or reproductive repercussions.

3.3.3. Molecular dynamic simulation

MD simulation studies substantially aid in understanding the link between the atomic-level ligand residues and the dynamics of protein structure (De Vivo et al. 2016). After the ligand–protein complex were virtually screened, the stability and receptor flexibility was evaluated using MD simulations running at nanosecond time scales.

To assess the accuracy and stability of the systems, 100 ns of MD simulation trajectories were analyzed. Fig. 4 shows the RMSD of 2-carene-HER2 complexes. Cα-RMSD rises up to 32 ns, and then it evidently increases once more at around 45 ns. The protein attached to the ligand stabilizes at 34 ns with a tolerable average RMSD of 2.5 ± 0.03 Å throughout the simulation. The ligand is maintained in the active region of the protein during the simulation, and the tolerable range for the RMSD of 2-carene in contact with protein is 0.3–1.2 Å until 20 ns, at which point it gradually rises to 2.8 Å. Fig. 5 shows the protein–ligand 2-carene-HER2 complex RMSF. From an atomic perspective, RMSF is between 0.5 and 4.0 Å. The average residue-wise RMSF remains between 2.0 and 2.5 Å, with larger peaks at the beginning (between 15 and 35 residues) and middle (between 150 and 200 residues). In Fig. 6, atom-by-atom RMSF of the protein in interaction with the ligand was displayed. Higher peaks, or loop regions, are flexible and reach a maximum of 4.0 Å. A crystal structure with some degree of thermal mobility is suggested by an average experimental (crystallographic) B factor of 3.52 Å. Protein structural mobility is revealed by the values of the B factors and RMSF at the residue level. The 2-carene-HER2 complex was shown to have a high affinity for protein binding in terms of binding energy, according to these results. In Fig. 7, interactions between proteins and ligands are compiled during the course of a 100 ns simulation. Hydrophobic contacts are formed by positively charged TYR-803 and LEU-852, and residues, including H-bonds, engage with ARG-811, THR-862, ASP-863, LEU-726, SER-728, and THR-811. Water bridges are formed by the residues ASN 850, LEU-807, GLY-804, and ASP-863, whereas negatively charged SER-728 and ARG-811 form ionic connections with 2-carene. Stability in simulation is represented by the interaction of 2-carene-HER2 complex complexes with the active site residues. Over 30.0 % of the simulation run time was devoted to protein–ligand interaction during MD simulation.

Table 1
Molecular interaction profile of ligand–protein complex.

Receptor proteins	*Van Der waals* Interaction	H Bonds	H-Bond Length (Å)	Hydrogen bond residues	pi-pi Interaction	Docking score (kcal/mol)
Estrogen receptor	TRP 383, ARG 394, LEU 349	3	1.069	ALA 351 TRP 383 GLU 353	ALA 350 LEU 387	−6.3
Progesterone receptor	LEU 718 THR 894	——	——	GLY 722 CYS 891	VAL 903	−6.3
HER2 receptor	SER 783, THR 798, ASP 863, LYS 753	4	1.613 1.770 2.435 1.7842	LYS 753 SER 783 MET 774 ASP 613	PHE 864 MET 774 LEU 785	−6.6

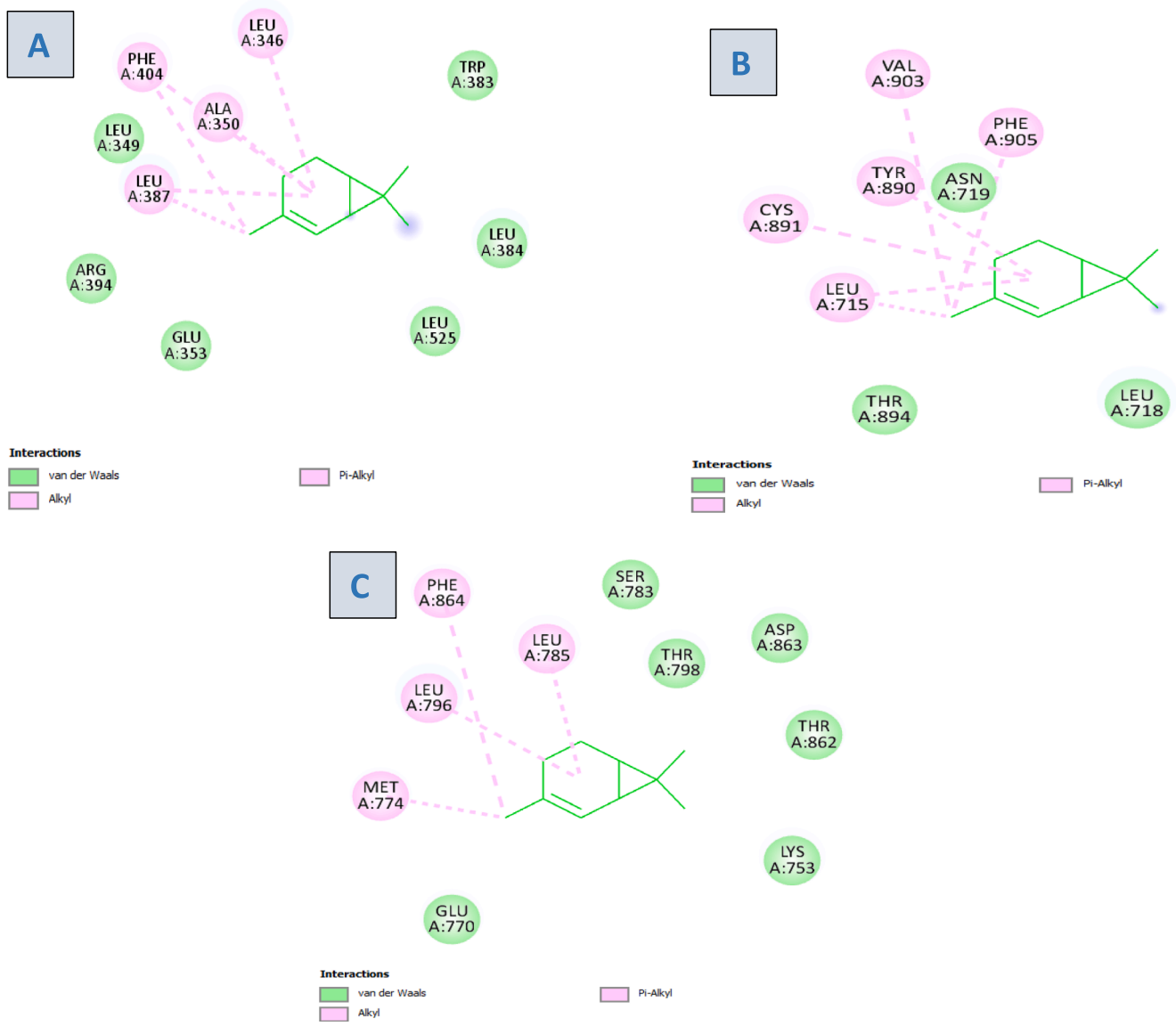

Fig. 2. 2D visualization of the ligand–protein complex with (A) Estrogen receptor (B) Progesterone receptor (C) HER2 receptor.

3.4. Nanoformulation characterization

3.4.1. Nanoemulsion encapsulation efficacy

The nanoemulsion mediated by terpene compound 2-carene has an entrapment efficiency (EE %) of 48.18 ± 0.88 percent. The entrapment efficiency is somewhat influenced by the concentration of the surfactant. Throughout the whole formulation process, the concentration of the surfactant and isolated component remained consistent. It was determined that an increase in viscosity was also responsible for the EE% rise based on data obtained from the EE% of prepared 2-carene based nanoemulsion. A higher concentration of surfactant or polymer causes the viscosity to rise, which improves the drug's integration into the generated nanoformulations by preventing the drug from diffusing into the exterior phase (Memar Bashi Aval et al. 2023). These results are also reported in literature presented by *Sharma et al*, 2014 (Sharma et al. 2014).

3.4.2. Nanoemulsion size and viscosity analysis

Nanoemulsions appear to be polydisperse and exhibit a wide variety of nanoparticular sizes. It was possible to see the average distinctive peaks at 295.6 nm of nanoemulsion (Supplementary Figure S8) respectively. The amount of oil phase and surfactant concentration in the nanoemulsion have a significant impact on the size of the nanoparticles. Tween 80 concentrations usually provide smaller droplet sizes due to increased stability. The PDI of NE was 0.389 was observed and showing homogeneity of particles. Zeta potential of monoterpene 2-carene mediated nanoemulsion, as evident from supplementary figure S9 is −9.74(mV). There is a single characteristic peak with 100 % area and Zeta deviation is 4.47 (mV) while conductivity of 0.351 (ms/cm) is observed. Table 4 shows viscosity and pH of nanoemulsion to check stability of prepared formulation.

3.4.3. UV–visible and FT-IR analysis

The UV–visible spectra of 2-carene, 2-carene with nanoemulsion, and EO revealed large absorption peaks along with a significant drop in intensity that occurred when the concentration of nanoemulsions in the sample was decreased. Absorption was also shifted to longer wavelengths. When the 2-carene curve was finally examined, the wavelength with the greatest peak, 482.6 nm, had an absorbance of 2.43. As the observed wavelengths comes within specified range so, confirmative to the formation of terpenes-based nano-emulsion formulation. The sharp maximum absorption peak at 530 nm (0.5 mg/ml of NE) and 505.6 nm

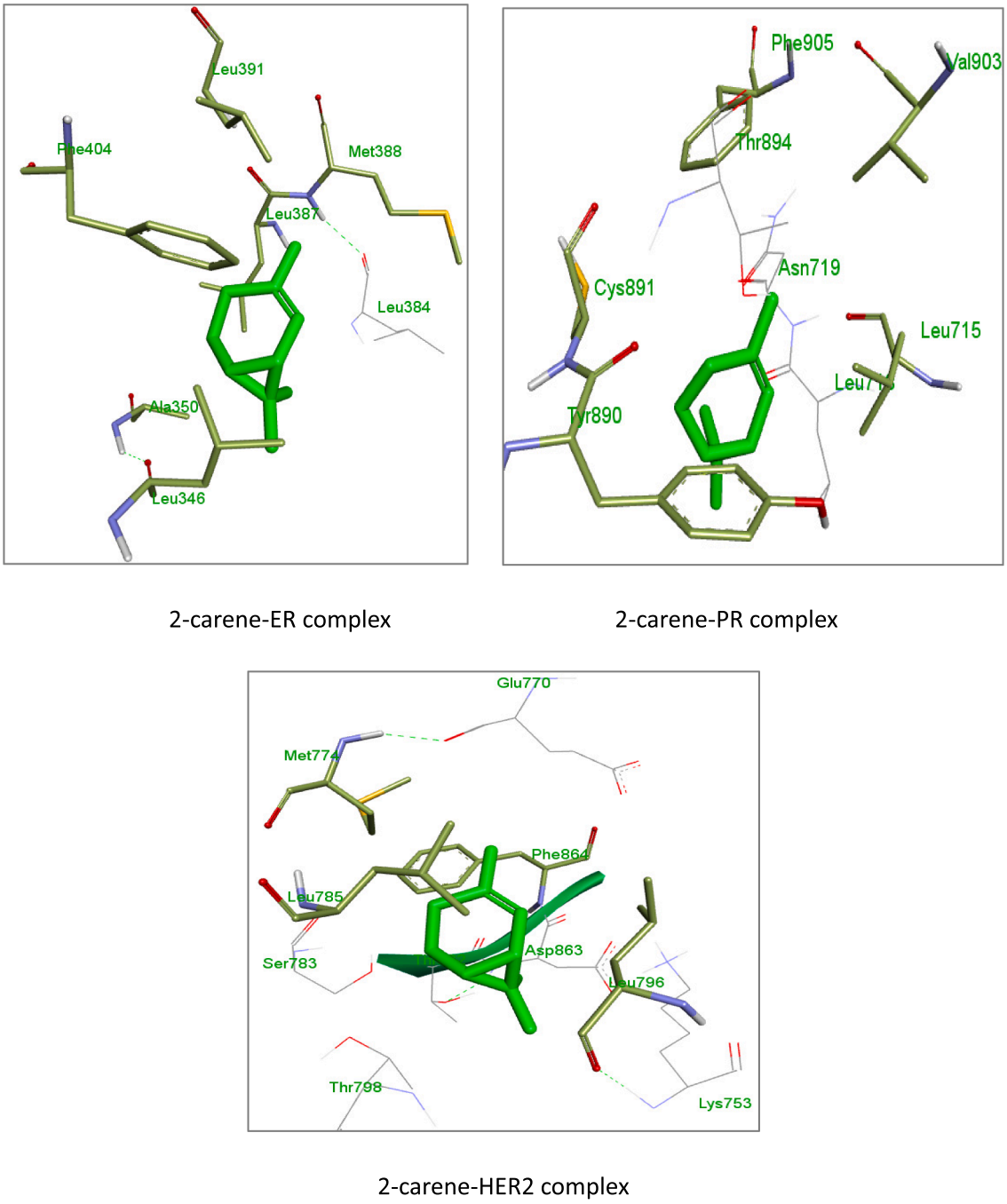

Fig. 3. 3D images of 2-carene with residual amino acids.

(1 mg/ml of NE) was an indicative of spherical shaped NPs respectively (Fig. 8).

The FTIR spectroscopic study of the nanoparticles was used to recognize functional groups that were likely in charge of reduction of different ions present in formulation. FTIR of nanoemulsion had been shown in Fig. 9 where values of wavenumber cm^{-1} had been plotted versus transmittance and spectral peaks were observed for NEs. There were numerous characteristic peaks observed at 3336.0 cm^{-1}, 2922.2 cm^{-1}, 1636.3 cm^{-1}, 1457.4 cm^{-1}, 1349.3 cm^{-1} 1086.5 cm^{-1} and 944.9 cm^{-1} as evident from FTIR plot of nanoemulsion of 2-carene. The vibrational peak around 3336.0 assigned to O–H that could possibly derive from carbohydrate or phenolics. The peak at 2922 cm^{-1} is ascribed to C–H of the alkyl group, the peak at 1636.3 cm^{-1} suggest C=O from carboxyl group or esters, the peak at 1086.5 cm^{-1} is likely due to C-O from phenols. The peak at 944.9 cm^{-1} possibly deviate from ether like groups and shown C-O-C stretching. The tentative assignment of the peak is supported by published literature reports.

3.4.4. SEM and EDX analysis

SEM examination was performed on the samples to ascertain the size distribution and morphology of the particles. The nanoemulsion imaging demonstrated that these were tiny globular shaped molecules, with an average diameter ranging from 180 to 270 nm. SEM scans showed that the 2-carene based nanoemulsion had randomly distributed, interconnecting nanoparticles. Because it allows for adequate medicine loading, the porosity structure of formulations is caused by the aromatic ring present in the monoterpene structure of 2-carene (Fig. 10). The emulsifying agents that were used during the formulation process may

Table 2
ADME profile of 2-carene.

ADME parameters	ADME score
MW	136.13 g/mol
nHet	0
TPSA	0.0
iLOGP	4.349
Flexibility	0.0
LOGS	−3.988
HIA	0.003
BBB penetration	0.517
PPB	90.10 %
GI absorption	High
Pgp substrate	0.006
CL	12.0
T1/2	0.125
hERG Blockers	0.032
CYP1A2 inhibitor	0.856
CYP3A4 inhibitor	0.04
CYP2C19 inhibitor	0.481
Bioavailability Score	0.55
PAINS alerts	0
Lipinski violations	1
Lead likeness violations	0

Table 3
Toxicity parameters of 2-carene.

Toxicity Parameters	Prediction value	Outcome
AMES toxicity	0.012	Mild toxic
H-HT	0.424	Moderately toxic
Rat oral acute toxicity	0.899	Highly toxic
FDAMDD	0.253	Positive
DILI	0.328	Mild toxic
Mutagenic	0 alert	No risk
Tumorigenic	0 alert	No risk
Acute toxicity	0 alert	No risk
Skin sensitization	0.443	Sensitizer
Carcinogenicity	0.063	Mild carcinogenic
Eye irritation	0.893	Irritant

have caused the nanoemulsion droplets to coalesce at a certain point, leading to the development of particles, as supported by previous studies (Giunti et al. 2019).

Using an EDX investigation, typical concentrations of C, O, S, Zn, and AU were found to be around 29.23, 21.55, 1.49, 11.15, and 1.2, respectively (Supplementary Figure S10). The spectral signals of sulfur (S) and carbon (C) also demonstrated the presence of biomolecules adsorbed on nanoemulsions. The presence of the OH group may also be indicated by the oxygen peaks as demonstrated by longer peaks observed from EDX of nanoemulsion.

3.5. DPPH antioxidant activity

The *in vitro* antioxidant activity of 2-carene and its nanoemulsion at different doses was evaluated using the DPPH technique (Fig. 11). 5 mL of methanolic solution (containing 0.2 mM of DPPH radicals) were mixed with 2-carene and varied doses of 2-carene mediated nanoemulsion. Terpene compound exhibited higher antioxidant activity compared to the nanoemulsion formulation. 2-carene demonstrated scavenging activity of 43 % to 57 % at concentrations ranging from 0.25 to 1 mg/mL, while nanoemulsion demonstrated scavenging activity of 24 % to 56 % with an average IC50 value of 0.72 ± 0.02. The DPPH activity of nanoemulsion increased in a dose-dependent manner, reaching its maximum at a concentration of 54.29 % at 1 mg/ml of nanoemulsion. However, the supreme antioxidant activity of 2-carene nanoemulsion was less than that ascorbic acid (used as standard), which was approximately 66 %. 1.5 mg/ml of nanoemulsion produced considerably stronger DPPH radical scavenging capabilities than all other all examined doses of nanoemulsions ($p < 0.05$).

3.6. Cytotoxicity assay

Using varying concentrations of tested substances (0.10 μg/ml, 0.25 μg/ml, 0.5 μg/ml, and 1 μg/ml) at multiple time intervals, the cytotoxicity of 2-carene and its nanoemulsion was examined. When applying 2-carene and biosynthesized nanoemulsion to MDA-MB-231 cancer cell lines and HMEpC healthy epithelial cells, the antiproliferative effect is contingent upon the duration and concentration of application. When compared to 51.62 % viability observed with nanoemulsion at a concentration of 1.0 μg/ml it was seen, cells that were treated with 2-carene shown highly significant p value ($p < 0.0001$). While pure 2-carene at 0.5 μg/ml showed significant cytotoxicity at $p < 0.0001$, the observed cytotoxicity was reduced at 0.25 μg/ml ($p = 0.0008$) (Fig. 12A). While nanoemulsion decreases cancer cell viability, cytotoxicity was found at concentrations of 1 μg/ml ($p = 0.0013$) and 0.5 μg/ml ($p = 0.005$) as compared to MDA-MB-231 control cell lines (Fig. 12B). With nanoemulsion, the maximum IC50 concentration with 1 μg/ml at 24 and 48 h, there was more than 50 % inhibition rate observed. As the concentration of nanoemulsion increased up to 1 μg/ml, the cytotoxicity was also raised substantially. Conversely, the HMEpC cells did not have any discernible impact on cell viability, with the exception of a $p = 0.007$ at a concentration of 1 μg/ml of nanoemulsion concentration.

In comparison to the viability of HMEpC cells, MDA-MB-231 cells

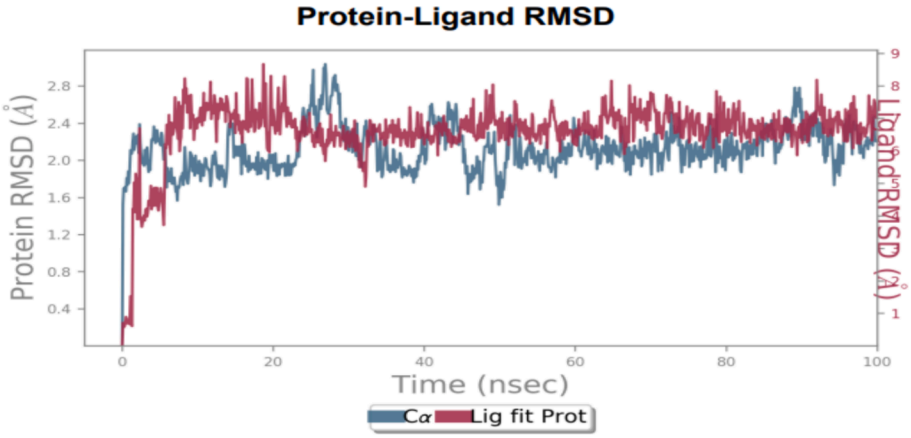

Fig. 4. RMSD of ligand 2-carene with HER2's C-atoms. The left Y-axis (blue line) displays the deviation in protein RMSD values, whereas right Y-axis (red lines) displays variance in ligand during the simulation. (For interpretation of the references to colour in this figure legend, the reader is referred to the web version of this article.)

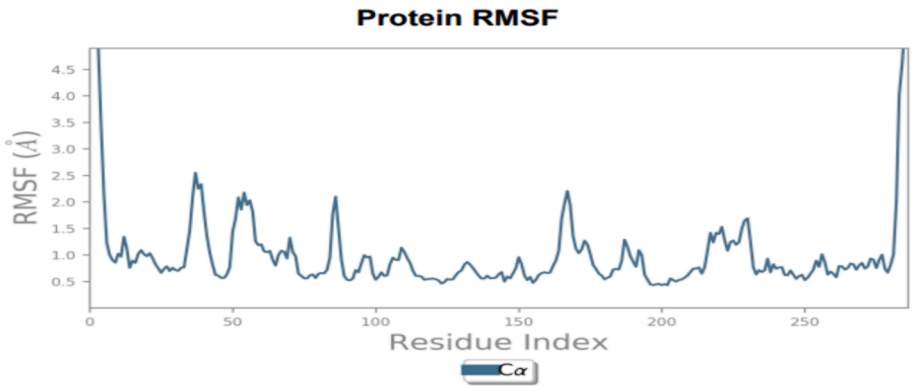

Fig. 5. Residue-wise RMSF of 2-carene with target protein HER2.

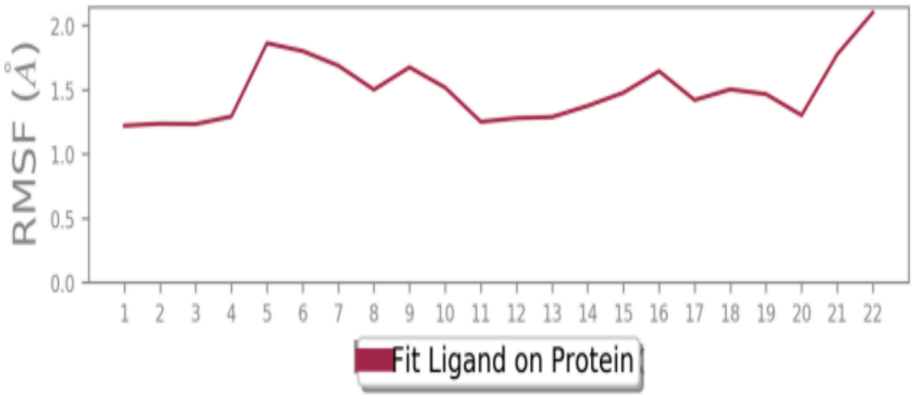

Fig. 6. Atom-wise RMSF of protein in contact with 2-carene.

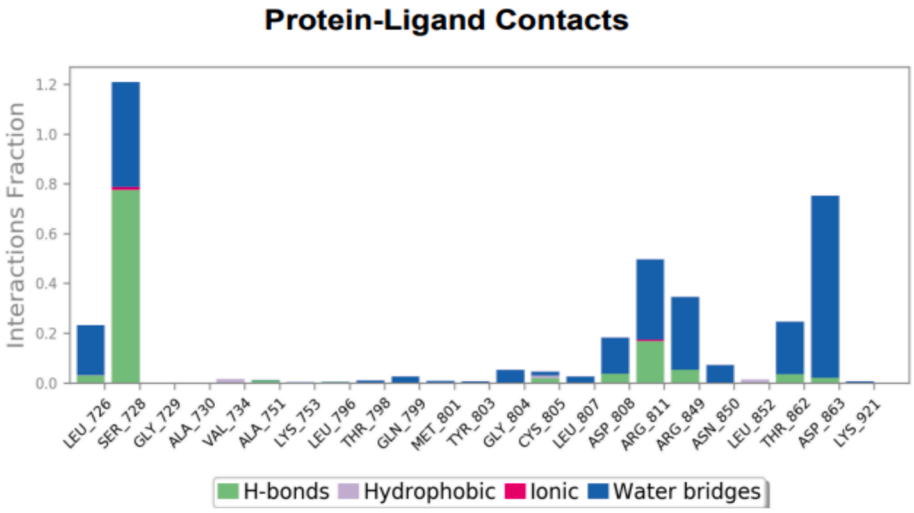

Fig. 7. Histogram characterize contacts between protein–ligand interaction during MD simulation.

Table 4
Dynamic Viscosity and pH of 2-carene Nanoemulsion.

Days	Viscosity (mPa.s.) ± SD	pH±SD
At Ist day	2.00 ± 0.10	5.87 ± 0.06
At 14th day	2.15 ± 0.10	5.93 ± 0.03
At 28th day	2.17 ± 0.21	5.93 ± 0.02
At 40th day	2.21 ± 0.20	5.98 ± 0.02

treated with 2-carene and at various doses of the nanoemulsion via crystal violet assay (live cells detection), displayed less live cells (Fig. 13). Nanoemulsion shown considerable cytotoxicity response ($p < 0.001$) on cancer cells, while 2-carene showed minimal absorption ($p < 0.001$) in comparison to untreated MDA-MB-231 cells. The viability of healthy HMEpC cells was found to be $p < 0.001$ when treated with 2-carene and $p > 0.005$ when treated with nanoemulsion concentrations in comparison to untreated control cells.

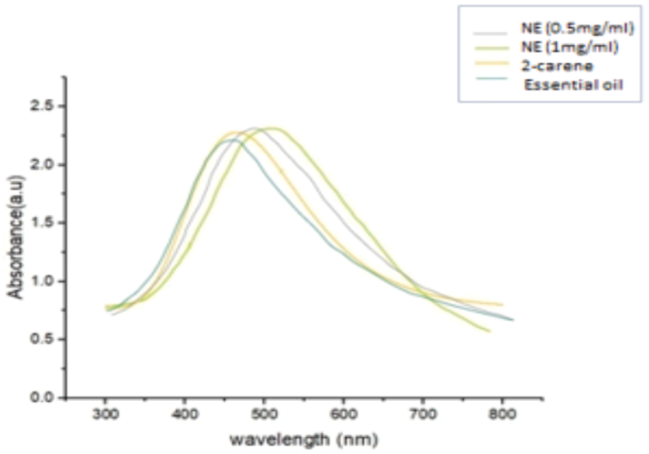

Fig. 8. UV–visible absorption spectrum.

3.7. Tumor growth rate

Effect of 2-carene and synthesized nanoemulsion was observed on tumor growth features. Average values of tumor length, tumor width and calculated tumor volume and tumor growth rate were mentioned by calculating tumor growth rate after administration of cancer and then treatment initiated with 2-carene and synthesized nanoemulsion in relevant groups. Rats in the DMBA control group had a higher tumor incidence than those in the vehicle control group ($p < 0.001$), despite not receiving any further nano-formulation treatment (Supplementary Table 5). In the groups treated with 2-carene ($p < 0.001$) and nano-emulsion ($p < 0.05$), there was a reduction in the incidence of tumors (Fig. 14). The groups treated with nanoemulsion showed a significant decrease in tumor size, with a tumor ratio of $p < 0.0001$ and a tumor ratio of $p < 0.001$ in the EO treated group, while the highest tumor ratio was found in the DMBA control group ($p < 0.0001$).

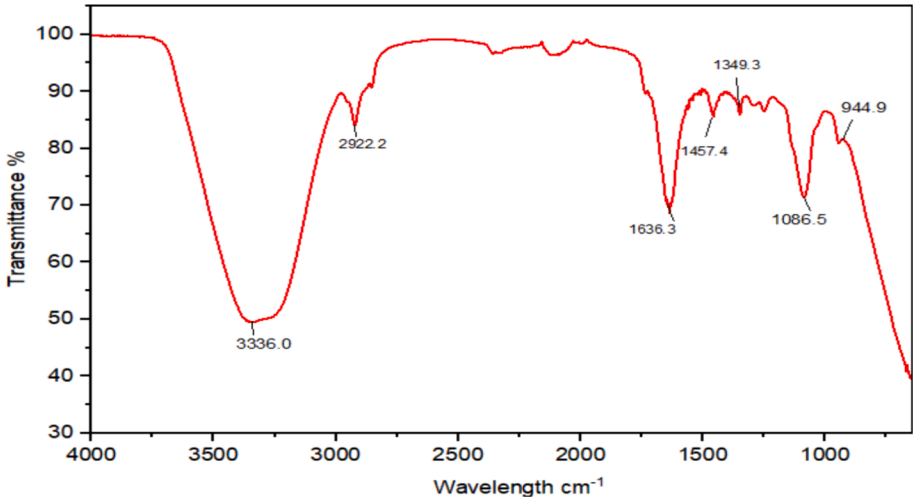

Fig. 9. FT-IR spectra of 2-carene mediated Nanoemulsion.

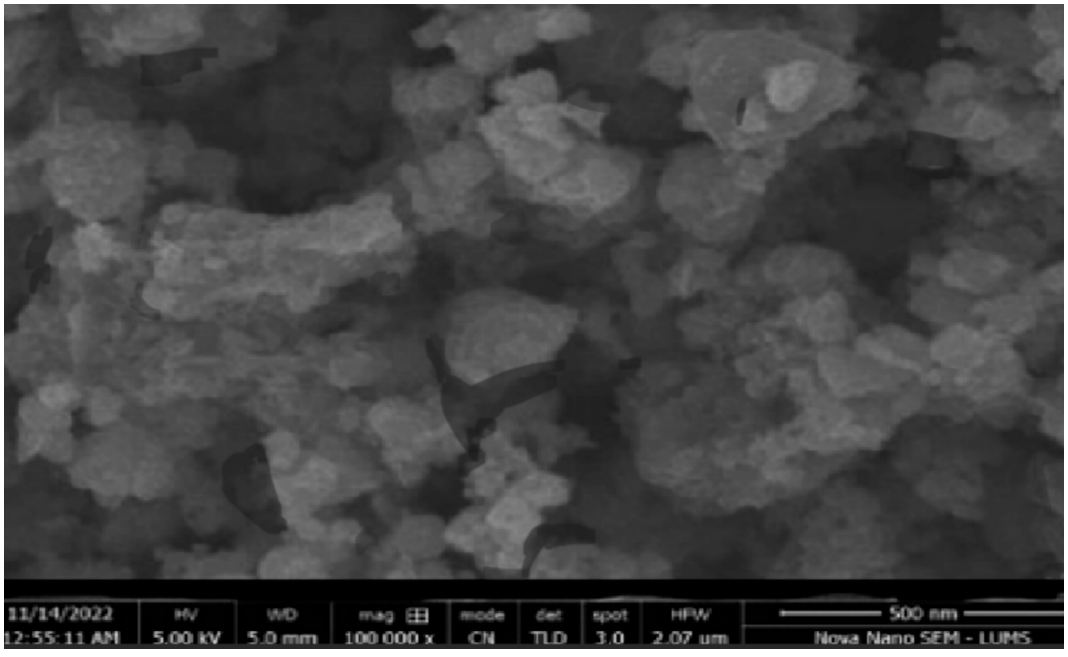

Fig. 10. SEM representation of 2-carene based Nanoemulsion.

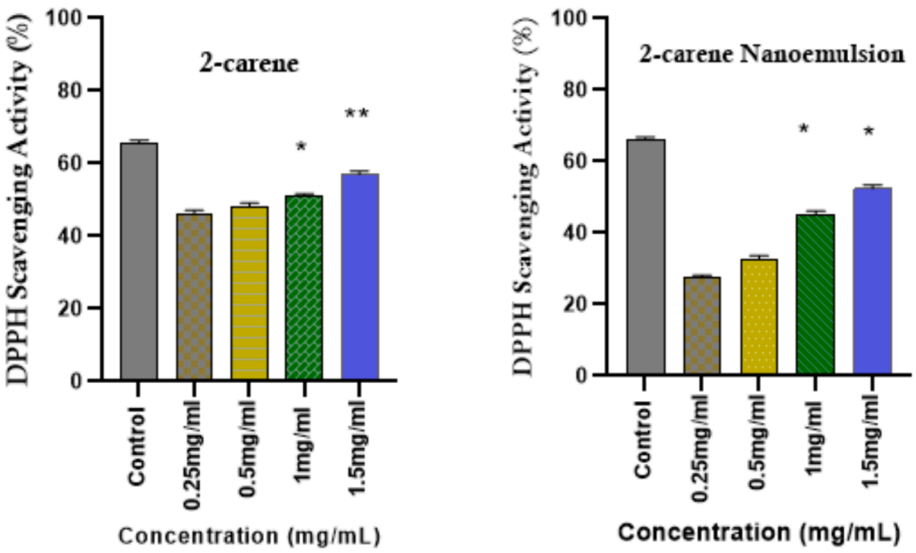

Fig. 11. DPPH radical scavenging activity of 2-carene and nanoemulsion. (The data represents statistical significance where *p < 0.05, ** p < 0.001, and *** p < 0.0001.

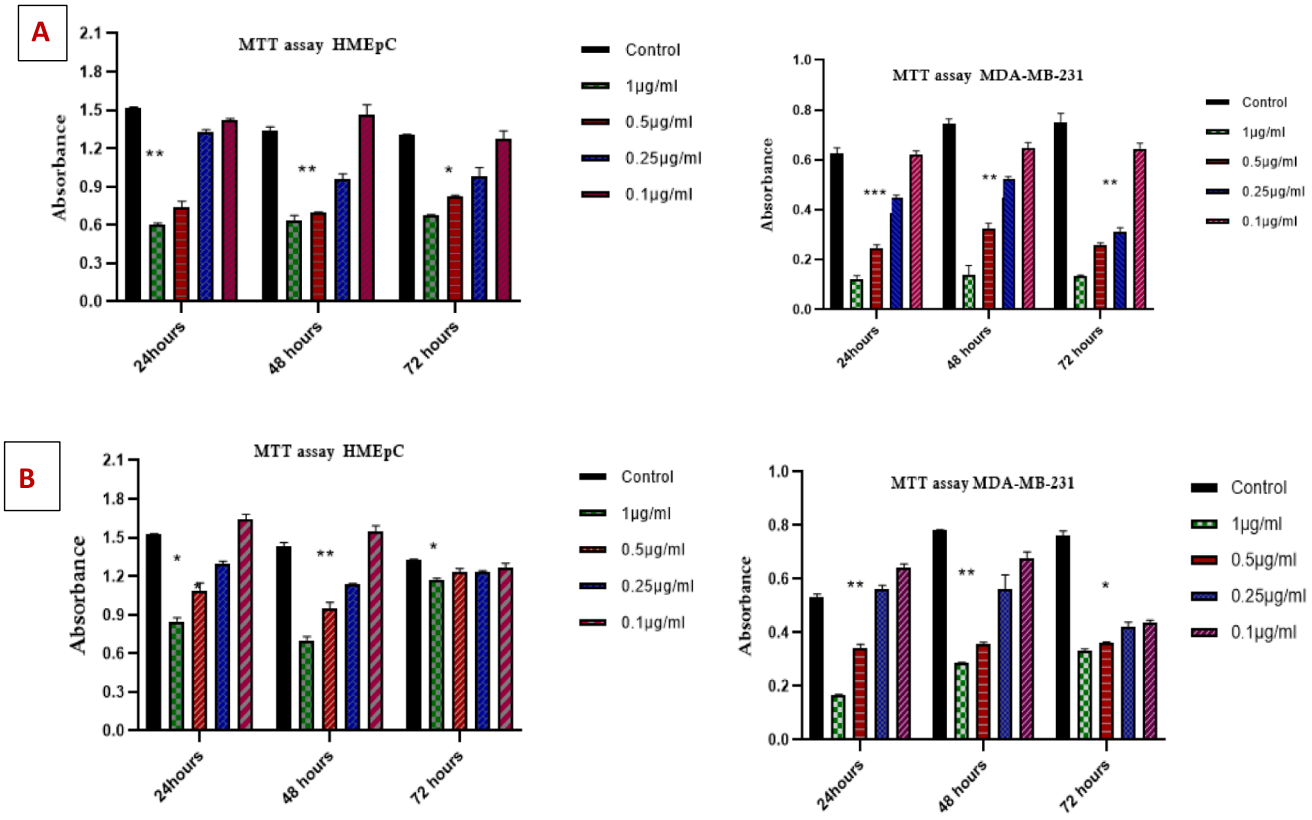

Fig. 12. MTT Cytotoxicity examination of (A) 2-carene and (B) nanoemulsion. The data displays the mean ± standard deviation, with * (p < 0.05), ** (p < 0.001), and *** (p < 0.0001) indicating statistical significance compared to vehicle group and DMBA induced group.

3.8. Apoptosis assay

Phytocompound's anti-tumor efficacy is determined through apoptosis, a programmed death process in cells brought on by pharmacological stimuli. The vehicle control group's apoptosis rate was suggestively lower (p < 0.0001) than that of 2-carene and bio-synthesized nanoemulsion treatment groups (Fig. 15). The vehicle control group had an apoptosis rate of 5.31 ng/ml, the nanoemulsion control group 5.28 ng/ml, the DMBA induced group 10.23 ng/ml, the 2-carene group 11.1 ng/ml, the nanoemulsion group 12.54 ng/ml, and the EO group 7.31 ng/ml, respectively. Significant apoptotic activity was renowned in cancer induced animals (which was not given nano-emulsion treatment); p = 0.0008. 2-carene mediated nanoemulsion revealed a greater number of significant apoptotic events (p < 0.001) in comparison to the control and DMBA cancer group.

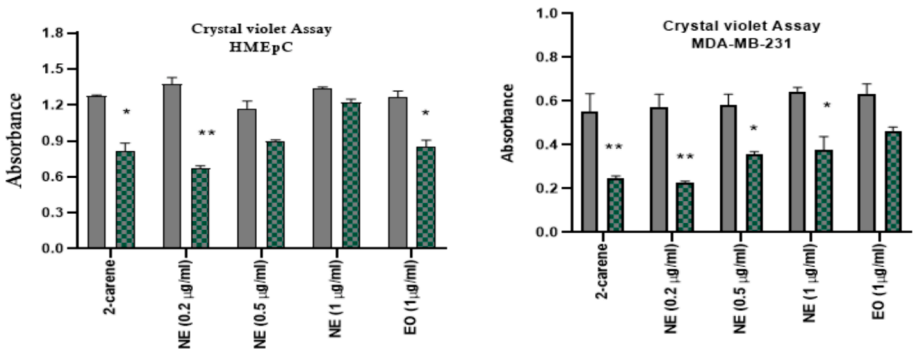

Fig. 13. Crystal violet cytotoxicity analysis of 2-carene and nanoemulsion. The data displays the mean ± standard deviation, with * ($p < 0.05$), ** ($p < 0.001$), and *** ($p < 0.0001$) indicating statistical significance compared to vehicle control group and DMBA induced group. (For interpretation of the references to colour in this figure legend, the reader is referred to the web version of this article.)

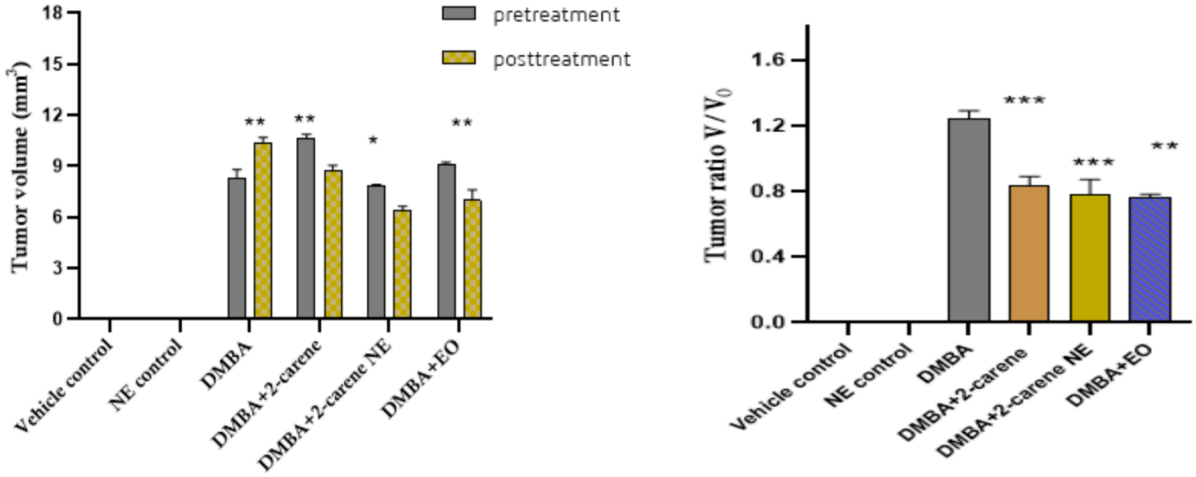

Fig. 14. Pretreatment and posttreatment tumor volume and tumor ratio V/V0. The data displays the mean ± standard deviation, with * ($p < 0.05$), ** ($p < 0.001$), and *** ($p < 0.0001$) indicating statistical significance compared to vehicle control group and DMBA induced group.

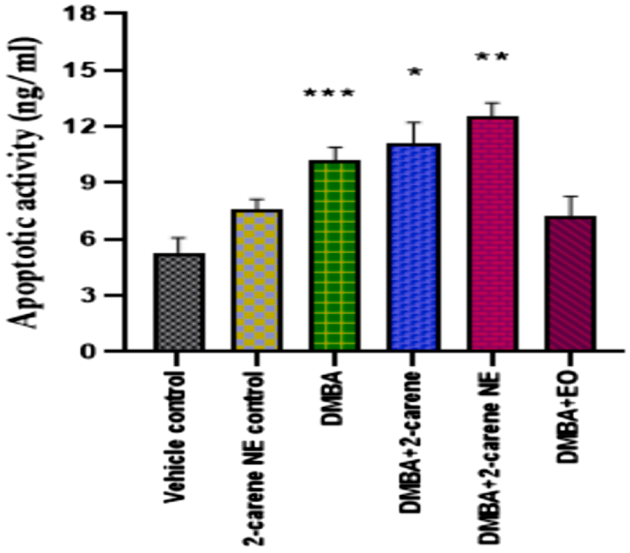

Fig. 15. Apoptotic analysis after administration of 2-carene and nanoemulsion. The data displays the mean ± standard deviation, with * ($p < 0.05$), ** ($p < 0.001$), and *** ($p < 0.0001$) indicating statistical significance compared to vehicle control group and DMBA induced group.

3.9. Inflammatory cytokine indicator analysis

Pro-inflammatory cytokines IL-1, IL-6, IL-23 and TNF-α were measured in DMBA induced cancer rats. A rise in the level of serum IL-1 ($p < 0.0001$) was observed in DMBA cancer induced rats as compared to vehicle control group. 2-carene treated group shown improvement in IL-1 level (25.21 pg/ml), where $p < 0.001$ and nanoemulsion treated group showed IL-1 level 36.22 pg/ml ($p < 0.05$) as compared to DMBA induced group which is statistically significant. 2-carene improve IL-6 level in DMBA induced rats as shown in Fig. 16. There was a significant difference ($p = 0.031$) in the levels of IL-6 between the nanoemulsion positive control group and the DMBA control group. Using NE treatment resulted in a substantial difference in IL-6 levels ($p = 0.0014$). When comparing DMBA-induced cancer-ridden rats to the vehicle control, a substantial increase in level of IL-6 was noted ($p < 0.001$). The DMBA-induced group treated with nanoemulsion showed a 56.14 ± 0.22 drop in IL-6 levels. The levels of IL-6 in animals treated with 2-carene and nanoemulsion significantly improve ($p < 0.001$). Additionally, the DMBA+EO treated group showed a significantly improved level ($p < 0.001$).

IL-23 was detected and a substantial rise in the level ($p < 0.0001$) was observed in DMBA cancer induced group in comparison to control groups. A substantial improvement was noticed in terpene compound treated group where $p = 0.015$ (p value was insignificant) as compared to DMBA untreated group, $p < 0.001$ in nanoemulsion treated group having IL-23 level (57.54 pg/ml) and a remarkable alteration was also observed in essential oil treated group ($p = 0.014$).

TNF-α levels were higher in the positive control group than in the

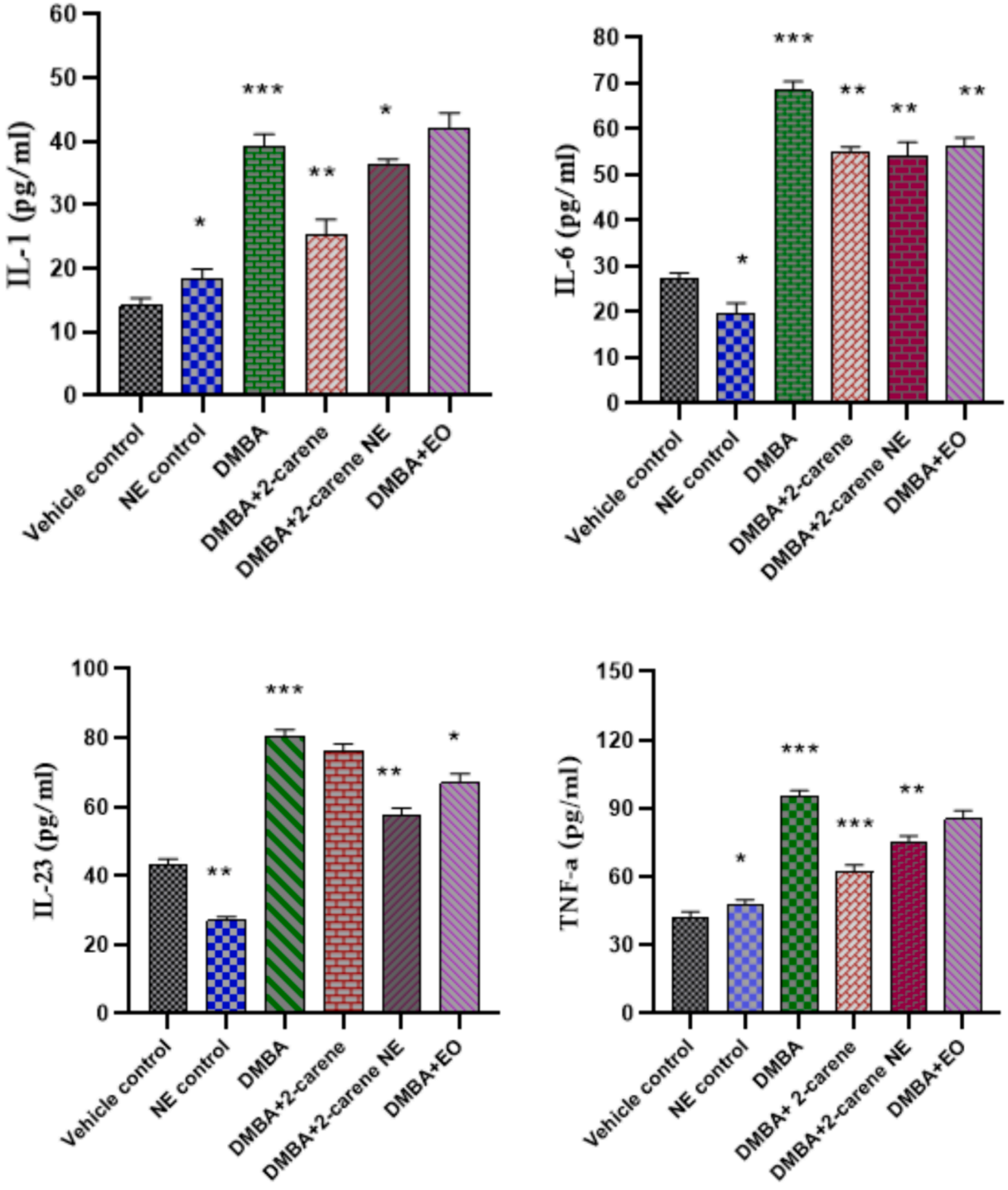

Fig. 16. Effect of 2-carene and nanoemulsion on inflammatory marker level. The data displays the mean ± standard deviation, with * ($p < 0.05$), ** ($p < 0.001$), and *** ($p < 0.0001$) indicating statistical significance associated to vehicle control group and DMBA induced group.

vehicle control group ($p < 0.05$). The DMBA-induced group showed elevated serum TNF-α levels (95.67 pg/ml), which was significantly different from the control animals ($p < 0.0001$) and the positive control group treated with nanoemulsion ($p < 0.001$). There was a statistically significant difference in the serum level of TNF- α (74.75 pg/ml) between the groups treated with 50 mg/kg of nanoemulsion and the untreated group produced cancer with $p < 0.001$. TNF-α in serum samples was significantly lower in the cancer-induced terpene treatment group (62.11 pg/ml) than in the untreated DMBA induced group ($p < 0.001$).

3.10. Hematological analysis

Following four weeks of 2-carene and nanoemulsion therapy in both control and DMBA induced rats, hematological examination revealed certain alterations in the experimental animals' blood profiles. In contrast to the control group, the DMBA cancer induced group (not treated by terpene or nanoemulsion) exhibited higher levels of platelets, WBCs, and RBCs, while the nanoemulsion treated group showed a significant decrease in WBCs ($p < 0.05$). The DMBA group exhibited a statistically significant increase ($p < 0.001$) in WBC counts when compared to the normal group. When compared to the DMBA group, the

administration of synthesized nanoemulsion in cancer-induced rats resulted in a significant ($p < 0.001$) decrease in red blood cells (RBCs) and platelets. While there was a decrease in hemoglobin levels in terpene treated and nanoemulsion treated groups but this difference was not statistically significant ($p > 0.05$). Compared to the DMBA-induced untreated group, 2-carene increased the platelet count ($p = 0.05$) and WBC count ($p = 0.062$). Neutrophils and monocytes were significantly higher in the terpene treated group and the nanoemulsion treated group compared to the control group ($p < 0.001$ and $p < 0.05$, respectively). According to Table 5 data, the rats' WBCs, TLC, and platelet profile were all considerably impacted by the 2-carene mediated nanoemulsion after they were given DMBA-induced cancer.

3.11. Oxidative stress marker analysis

It is essential to detect level of antioxidant enzymes developed due to DMBA induction and then evaluate effect of pure isolated compound 2-carene, EO and nano-emulsion on different stress markers. Increased level of SOD enzyme was observed in DMBA control group ($p < 0.05$) compared to the vehicle control group. Group treated with nano-emulsion displays $p < 0.001$. As it was demonstrated that, in comparison to DMBA-induced rats who were not treated, SOD concentration markedly increased in rats that had been given nanoemulsion treatment where $p = 0.0012$ and this differene was significant and group treated with 2-carene treatment shown decrease in SOD level ($p > 0.05$).

When comparing the 2-carene and EO treated groups to the untreated DMBA group (untreated group), the CAT level dropped in both cases ($p < 0.05$ and $p < 0.001$). The 2-carene treated group's CAT level, which was 21.02 ± 0.14 Unit/mg, improved. The untreated group induced with DMBA had the highest CAT level, at 28.41 ± 0.12 Units/mg. In comparison to the DMBA-induced cancer control group, CAT values in the nanoemulsion treated groups were found to be $p = 0.041$ (Fig. 17).

GPx activity was observed in the DMBA induced group ($p = 0.0001$) relative to the control group. In comparison to the control group, the nanoemulsion treatment group exhibits significant values ($p < 0.05$), but GPx value observed in the EO treated group was also statistically significant ($p = 0.0014$). As in contrast to the vehicle control group, the DMBA-induced and treated groups had higher GPx concentrations ($p < 0.05$) and rats with DMBA-induced cancer afterward treated with 2-carene and 2-carene mediated nanoemulsion dramatically raised GPx activity ($p < 0.001$) in comparison to vehicle control group but markedly shown improvement in GPx levels after nanoemulsion treatment suggesting that 2-carene based nanoformulation may have a positive impact on glutathione peroxidase levels.

GSH levels were monitered in rats in all experimental groups and DMBA induced animals exhibited a substantial ($p < 0.0001$) reduction in glutathione levels (18.11 ± 2.06 Units/g) compared to the vehicle control group of rats. In the DMBA-induced group, nanoemulsion administration raised the level of GSH (18.43 ± 2.06 Units/g) in contrast to DMBA induced untreated group, although this difference was not statistically significant ($p > 0.05$). Although rats treated with EO fter cancer induction shown a substantial improvement in GSH level where $p < 0.05$ (Fig. 17).

3.12. Histopathology of mammary cancer

Sections of the control group's mammary tissue that had been H&E stained showed normal morphology. Histopathological alterations were not observed in the emulsion control or vehicle control groups (Fig. 18 A and B). Histopathology determined that the tumor type in DMBA-treated groups was a differentiated adenocarcinoma. Cribriform adenocarcinomas, characterized by abnormal cell development, hyperplasia with dilated ducts, and a little amount of fatty tissue, were found in rats with mammary tumors in the DMBA induced group (who were not treated with terpenes or nanoemulsions). Adipose tissue invasion were present in the solid tumor in the DMBA group. Animals with cancer developed proliferative lesions and lobular hyperplasia. Comparing the DMBA group to the terpene 2-carene group, there was a minor decrease in the tubular structures and surrounding fibrosis. The DMBA+nanoemulsion group included a wide range of nuclei and exhibited very minimal ductular growth. But the group receiving nanoemulsion treatment also had some degree of fibrosarcoma (Fig. 18 E). Analyzing the mammary tumors in rats with nanoemulsion indicated the presence of an adenocarcinoma, corroborated by a slight damage of the parenchyma and mammary cells. Rats with breast tumors can have their hyperproliferation reduced by a particular dose of nanoemulsion administration, which is crucial for prolonging the survival of the rats.

4. Discussion

2-carene is a monoterpenoid phytocompound and it was investigated to evaluate its cytotoxic and anti-proliferative effects against breast cancer by formulating nanoemulsion of this compound. As many terpenes, triterpenes and terpenoids, which are important components of essential oils, have been found to be plentiful in plant extracts and to have anti-tumor, anti-inflammatory, apoptotic, and antioxidant properties. In order to create a biosynthesized nanoemulsion of this isolated, pure chemical for efficient nano-based drug delivery, it was crucial to study its impact in breast cancer model. It was recommended that this isolated compound was investigated by *in silico*, *in vitro*, and *in vivo* studies on BC because there were no conclusive results found in previous reported literature about the anticancer potential of 2-carene based nanoemulsion in cancer model. Our investigation confirms that the formulated nanoemulsion has anti-oxidative and anticancer effects. As some of the phytocompounds found in *C. roseus* are effective in treating

Table 5
Effect of 2-carene and synthesized Nanoemulsion on hematological parameters.

Parameters	Vehicle control	Nanoemulsion control	DMBA control	DMBA+2-carene	DMBA+2-carene nanoemulsion	DMBA+EO
RBCs ($\times 10^6$ / μL)	7.24 ± 0.05	7.81 ± 0.08	10.22 ± 0.13	8.82 ± 0.11*	9.45 ± 0.54**	10.43 ± 0.33
WBCs ($\times 10^3$ / μL)	11.11 ± 0.21	13.44 ± 0.81	17.42 ± 0.22**	13.41 ± 0.87	14.33 ± 0.76*	13.76 ± 0.77
Platelets ($\times 10^3$ /μL)	930.00 ± 13.01	1211 ± 11.8	1711 ± 12.8	1476 ± 11.9	1567 ± 12.8**	1598 ± 13.98
TLC ($\times 10^3$ /μL)	8.11 ± 0.16	7.37 ± 0.14	13.11 ± 0.81	9.34 ± 0.76	12.55 ± 0.12	14.65 ± 0.17**
Hb (g/dL)	13.12 ± 0.31	13.0 ± 0.21	18.7 ± 0.22**	14.3 ± 0.32	12.8 ± 0.17	17.5 ± 0.71
Neutrophils (%)	22.50 ± 2.12	33.1 ± 2.11	31 ± 2.72**	35 ± 2.01**	31 ± 2.32	28 ± 2.16
Monocytes (%)	2.13 ± 0.22	3.11 ± 0.10	4.2 ± 0.42	4.0 ± 0.32**	3.01 ± 0.99*	3.16 ± 0.51*

Results expressed in mean ± standard and n = 7. Mean having *($p < 0.05$), ** ($p < 0.001$), ***($p < 0.0001$) are statistically significant paralleled with control groups.

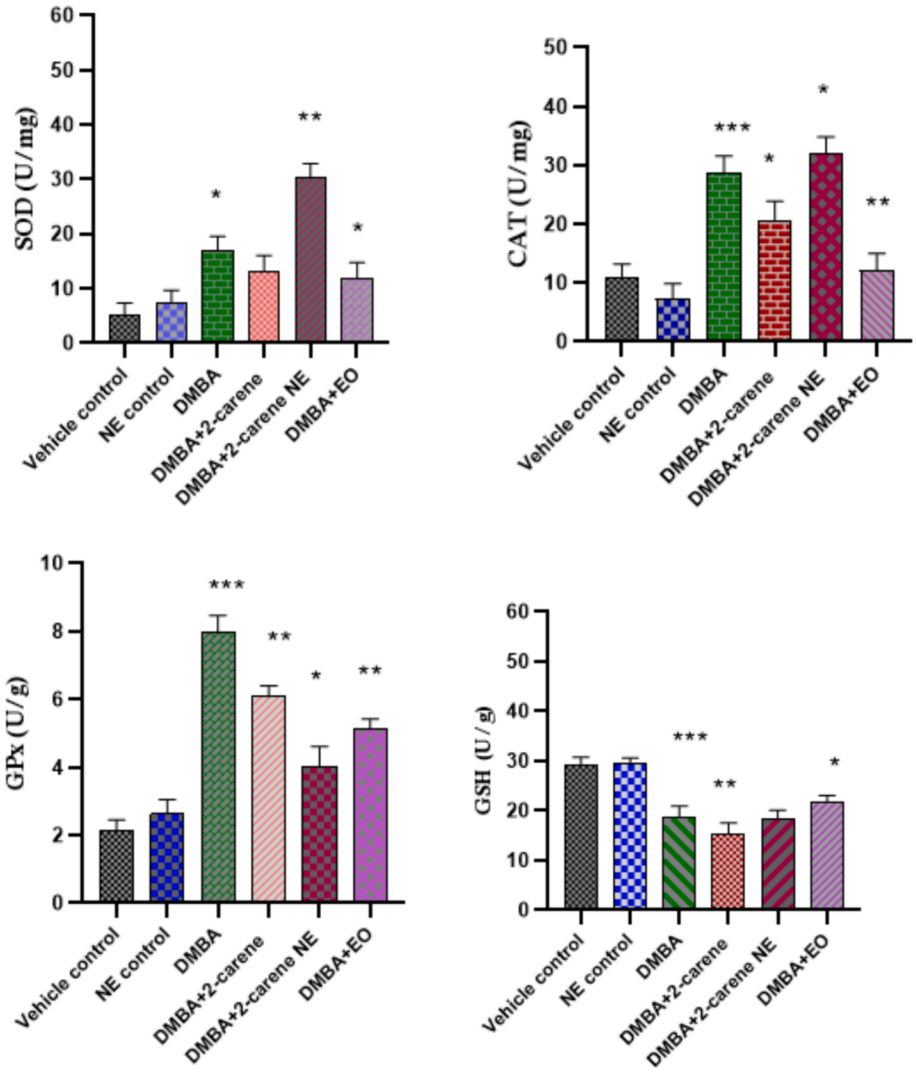

Fig. 17. Effect of 2-carene and nanoemulsion on oxidative stress enzymes. The data displays the mean ± standard deviation, with * ($p < 0.05$), ** ($p < 0.001$), and *** ($p < 0.0001$) indicating statistical significance compared to vehicle control group and DMBA induced group.

cancer, inflammatory illnesses, genitourinary system disorders, liver, and prostate disorders (Kumar, Singh, and Singh 2022). Most of plant species are generally capable of producing a large variety of phytochemicals. *Catharanthus roseus* contains flavonoids, terpenes, and alkaloids such as vincristine, vinblastine, catharanthine, ajmalicine, vindolicine, and vindoline (Thulasidas, Sadasivam, and Varadarajan 2019). Essential oil reduced oxidative stress levels, inflammatory interleukins, and tumor growth rate due to existence of terpene phytocompounds in medicinal agents (Rojas-Armas et al. 2022). *C. roseus* plant was selected due to its recommendation in various studies, as it was acclaimed that as compared to the control group, kidney metabolites and liver enzyme activity were significantly lower in a dose-dependent pattern when the ethanolic extract of *C. roseus* was administered. The findings imply that oral administration of the ethanolic *C. roseus* extract does not adversely affect the kidney or liver in Wistar rats, and in fact, may even improve the organs' functional characteristics (Adekomi 2021). At 300 mg dosages, there was an improvement shown in biochemical and acute toxicity profiles of rats treated with *C.roseus* extract. More than 300 mg of *C. roseus* extract can cause biochemical and histological toxicity in the liver, kidney, and heart. It is advised that treatment be administered at doses lower than those that were investigated (Vutukuri et al. 2017).

Terpenes, triterpenes, monoterpenes, flavonoids, and saponins are abundant in *C. roseus* (Lawal et al. 2015). Natural phytocompounds have been demonstrated to offer therapeutic advantages in a range of pathophysiological conditions, such as immune-compromised disorders, malignancies, and inflammatory illnesses (Emtiazi et al. 2022). It is thought that monoterpene and monoterpenoids can be used as a molecular platform to create novel medications and cancer medicines (Il'ina et al. 2020). Geraniol is a monoterpene, tested against hepatic cancer cells and it helps to stop the growth of breast and liver malignant cells (Thoppil 2011). In accordance with the present study it was concluded that when combined with traditional chemotherapy, nano-based phytochemical formulations have shown promising results in cancer treatment, with fewer side effects and increased efficacy (Emtiazi et al. 2022). It has become more popular to create phytochemical based nano-formulations in order to maximize their therapeutic potential by enhancing their bioavailability and target specificity (Singh et al. 2019).

Cancer was shown to have elevated levels of chronic inflammatory and oxidative stress markers, similarly to those observed in our study. An additional effect of oxidative stress in cancer patients was more significantly mediated by an increase in oxidative enzymes than by inflammatory indicators (Heidari et al. 2019). Likewise, as observed in our study, oxidative stress enzymes were elevated in DMBA cancer induced group after cancer induction as compared to control groups ($p < 0.001$), a research has also shown that oxidative stress causes oxidative enzymes

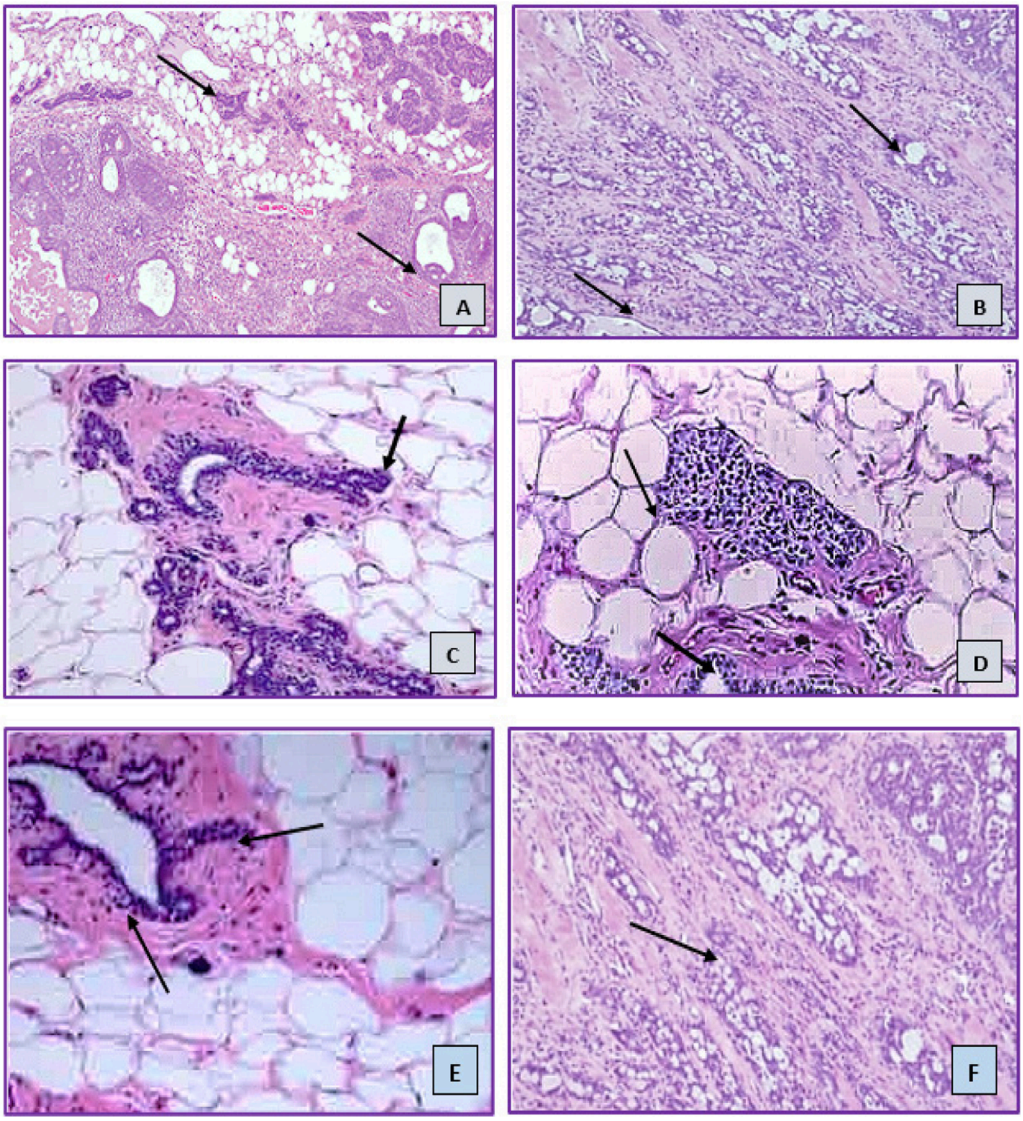

Fig. 18. Histology images of (hematoxylin and eosin) of mammary gland tissues. (Here A: control group; B: Nanoemulsion control; C: DMBA induced untreated group; D: 2-carene treatment; E: 2-carene mediated nanoemulsion treatment and F: Essential oil treatment group).

to be triggered in BC cells, and it is well known that ROS is produced by DMBA-induced cancer and plays a part in some tumor development (Arfin et al. 2021). Terpenes and terpenoids are helpful in a range of cancer treatments because of their cytotoxic and anti-proliferative qualities. Terpenes, triterpenes, and monoterpenoids are important constituents of essential oils and are abundant in plant extracts, exhibiting apoptotic, anti-cancer, and antioxidant effects (Barras, Ling, and Rivas 2024). In accordance with our findings, it was investigated that the antioxidant properties of *H. sabdariffa* calyxes were due to the presence of alkaloids, terpenes, and vitamins. Anokwuru et al. demonstrated that the majority of antioxidant activity of the *H. sabdariffa* extract and its nanoformulations is accounted. At 125 mg/kg, the SOD activity levels of the *H. sabdariffa* extract under investigation rose while the MDA level dropped (Anokwuru et al. 2011).

In a reported study, a compound identified as, 3-Carene is also similar type of monoterpene that is found naturally in many different types of plants. Its antibacterial, cytotoxic, and therapeutic properties are yet to be investigated (Ren et al. 2022) and (Shu et al. 2019). Data recommended that α-pinene, a monoterpene compound has strong cytotoxic capability and can prevent cancer. α-pinene significantly inhibited cancer cell spread and induced cell cycle arrest. In xenograft tumors, α-pinene therapy induced apoptosis, and findings indicated that this monoterpene inhibits the growth of cancer and functions as an operational therapeutic agent for cancer treatment. (Zhao et al. 2018). Among the many remarkable biological actions exhibited by the monoterpenes and meroterpenoids, some terpene compounds also shown antioxidant and anticancer capabilities. For millennia, natural resources have played a crucial role in the advancement of human health and continue to be a priceless source of inspiration (Barras, Ling, and Rivas 2024). These substances have the potential to be developed into medicines, according to biological assessments. Terpenes isolated from essential oils have demonstrated anti-proliferative, anti- oxidant and antibacterial action against some clinical strains and have demonstrated encouraging outcomes against dozens of cancer cell lines(Mohamed Abdoul-Latif et al. 2022).

Phytochemicals mediated nanoformulations have potential anti-inflammatory and anticancer activities come from various plants and have a variety of chemical compositions. It was observed in present study that inflammatory cytokine levels measured after treatment with 2-carene and nanoemulsion and were improved in cancer induced animals ($p < 0.05$). These observations are supported by a study reported that cineole a terpene compound, was also discovered to have a considerable inhibitory effect on pro-inflammatory factors including TNF-α and IL-1 (Madka and Rao 2013). In order to improve the efficacy

of certain bioactive compounds, such as curcumin, as cancer preventive medications, their bioavailability and absorption must be improved by formulating nano based formulations (Bezerra et al. 2006). Another study reached similar conclusions as ours study and stated that terpene phytochemicals have chemo-preventive characteristics because they decrease cancer cell growth, downregulate estrogen receptor expression, and induce apoptosis in tumor cells, which stops the cell cycle (Hussain et al. 2022). The spearmint oil and surfactants may have interacted specifically to form the stable nanoemulsion, which had the strongest lethal effect on cancer cells. Comparisons were made between the effects of excipients on the nanoemulsions' droplet size, oil phase content, and cytotoxic action. The intrinsic apoptotic pathway, which was the preferred route for potential anticancer drugs, can be evaluated by the use of spearmint oil-mediated nanoemulsion against cancer cells. By carefully choosing the type of essential oils, or phyto-compound, nanoemulsions that were cytotoxic to cancer cells were effectively used to suppress cancer cells growth (Tubtimsri et al. 2021).

As reported in a study, carotenoid nanoemulsion derived from sweet potato peel was able to efficiently demonstrate potential against breast indicators by inhibiting MCF-7 cell lines and lowering the rate of tumor growth. The potential anti-tumor efficacy could stem from the synergistic interaction of β-carotene and carotenoids in nanoemulsion, which effectively targeted cancer cell lines (Hsu and Chen 2022). Some terpenes found in coriander EO, like linalool, α-terpinene and α-pinene, have also been proven to have anti-inflammatory properties be able to reduce oxidative stress and cellular inflammation in chemically generated cancer (Abbas et al. 2022). Glycyrrhizic acid, carotenoids and oleanolic acid are triterpenoids with anti-tumor properties. These phytocompounds may start several pro-apoptotic signaling cascades that cause cancer cells to undergo apoptosis. The chemoprotective and chemopreventive properties of these chemicals suggest a possible use for them in contemporary anticancer therapy (Kuttan et al. 2011). The biochemical parameters of animals treated with compounds containing plants showed varying degrees of improvement. According to the research, certain phytocompounds made from plant parts could be employed as an easily accessible therapy for abnormal kidney biochemical parameters (Parthasarathy and Evan Prince 2021). Premedication with terpene mixtures increased SOD, CAT, IL-10, and brain-derived neurotrophic factor levels while tumor necrosis factor-alpha, malondialdehyde levels declined (Marefati et al. 2021). Terpenes resulted in cancer cell death around the site of damage in macrophages and lessened the production of inflammatory interleukins and TNF-α levels, resulted to minimize the inflammatory activity in cancer cells (Moussaieff et al. 2008). The terpene components menthone and camphane, which were added to the dosage form nanoemulsions, further increased the anticancer capabilities of *Mentha piperita* EO, and the effect obtained from NE of *M. piperita* essential oil was higher than that of *M. piperita* extract (Abedinpour et al. 2021). Noteworthy dose and time dependent anti-tumor properties were also seen in breast cancer cells 4 T1 by the administration of Pequi oil nano-emulsion (Ombredane et al. 2020). The administration of nanoformulations improves treatment efficacy by facilitating drug- delivery to specific sites and direct release into cancer cells. Medications delivered by incorporating as nanomedicine can be more effectively used and thanks to engineered nanoformulations, which also increase patient lifespan and well-being (Ganesan et al. 2021).

5. Conclusion

Many diverse plants and medicinal herbs naturally contain terpenes and terpenoids, some of which are effectively utilized in nanomedicines. This work presented the anticancer potential of nanoemulsion synthesized by using 2-carene. Computational analysis and interaction between 2-carene and breast cancer target proteins using molecular docking and ADMET profiling was remarkably observed. Docking studies anticipated the binding cavities of breast cancer receptors to observe the highest binding affinities. HER2 has the best docking contact with 2-carene, according to the docking research of all complexes. The considerable sustained *in-vitro* anticancer activity of the nanoemulsion against breast cancer cell lines was demonstrated by MTT assay. The synthetic formulation's and 2-carene's efficacy against DMBA-induced breast cancer was also assessed. In summary, it was determined that biosynthesized nano emulsions possess the capability to be utilized in focused cancer indication treatment and exhibit specific anticancer effects. Extensive preclinical studies of absorption, pharmacodynamics, biomarkers, and tumor suppression measures are necessary given the potency of 2-carene-mediated nanoemulsion.

Ethical approval

This study was previously approved by Institution of Molecular Biology and Biotechnology, Bioethical, Biosafety and Biosecurity Committee of Department of Molecular Biology and Biotechnology, University of Lahore with reference number CRiMM/23/Research/32 and is in accordance with research guidelines of IMBB, TUOL.

Authors contribution

Conceptualization, Writing original draft preparation, Iffat Nayila; Resources, Riaz Ullah and Tahir Maqbool; Data curation, Review and Editing, Sumaira Sharif, Madeeha Shahzad Lodhi and Amal Alotaibi; Supervision, Project administration, Sumaira Sharif and Saima Hameed. All authors have read and agreed to the published version of the manuscript.

CRediT authorship contribution statement

Iffat Nayila: Writing – original draft, Conceptualization. **Sumaira Sharif:** Supervision, Formal analysis. **Madeeha Shahzad Lodhi:** Resources, Formal analysis. **Riaz Ullah:** Resources, Formal analysis, Funding acquisition. **Amal Alotaibi:** Formal analysis, Funding acquisition, Resources. **Tahir Maqbool:** Resources. **Saima Hameed:** Visualization, Validation.

Declaration of competing interest

The authors declare that they have no known competing financial interests or personal relationships that could have appeared to influence the work reported in this paper.

Data availability

Data will be made available on request.

Acknowledgment

Authors wish to thank Princess Nourah bint Abdulrahman University Researchers Supporting Project number (PNURSP2024R33), Princess Nourah bint Abdulrahman University, Riyadh, Saudi Arabia for financial support.

Appendix A. Supplementary material

Supplementary data to this article can be found online at https://doi.org/10.1016/j.arabjc.2024.105937.

References

Abadi, Atena Vafaei Malek, Ehsan Karimi, Ehsan Oskoueian, Ghasem Rahimi Kalateh Shah Mohammad, and Negin Shafaei. 2021. Synthesis, characterization and cytoxicity evaluation of syzygium aromaticum l. bud (clove) essential oil nanoemulsion. In Review. preprint. doi:10.21203/rs.3.rs-952488/v1.

Abbas, A., Anwar, F., Ahmad, N., Shahid, M., Al-Mijalli, S.H., Yaseen, M., Farooq, S., Iqbal, M., 2022. Characterization of bioactives and nutra-pharmaceutical potential of supercritical fluid and hydro-distilled extracted coriander leaves essential oil. Dose-Response 20 (4). https://doi.org/10.1177/15593258221130749, 15593258221130749.

Abdoul-Latif, M., Fatouma, A.E., Merito, A., Nour, M., Risler, A., Ainane, A., Bignon, J., Ainane, T., 2022. Chemical analysis of essential oils of cymbopogon schoenanthus (L.) spreng. and nepeta azurea R.Br. Ex benth from djbouti, In-Vitro cytotoxicity against cancer cell lines and antibacterial activities. Appl. Sci. 12 (17), 8699. https://doi.org/10.3390/app12178699.

Abedinpour, N., Ghanbariasad, A., Taghinezhad, A., Osanloo, M., 2021. Preparation of Nanoemulsions of Mentha Piperita Essential Oil and Investigation of Their Cytotoxic Effect on Human Breast Cancer Lines. BioNanoScience 11 (2), 428–436. https://doi.org/10.1007/s12668-021-00827-4.

Adekomi, D. A. 2021. "Madagascar Periwinkle (Catharanthus Roseus) Enhances Kidney and Liver Functions in Wistar Rats." *International Journal of Biomedical and Health Sciences* 6(4). http://ojs.klobexjournals.com/index.php/ijbhs/article/view/665 (May 1, 2024).

Aebi, Hugo. 1974. "Catalase." In *Methods of Enzymatic Analysis*, Elsevier, 673–84. doi: 10.1016/B978-0-12-091302-2.50032-3.

Agrawal, H., Mishra, A., 2017. A study on influence of density and viscosity of emulsion explosive on its detonation velocity. Modell. Meas. Control C 78 (3), 316–336. https://doi.org/10.18280/mmc_c.780305.

Anokwuru, Chinedu, Godswill Anyasor, Ajibaye Olusola, Fakoya O., and Okebugwu P. 2011. "Effect of Extraction Solvents on Phenolic, Flavonoid and Antioxidant Activities of Three Nigerian Medicinal Plants." Nat. Sci. 2011;*9(7)* 9: 7.

Arfin, S., Jha, N.K., Jha, S.K., Kesari, K.K., Ruokolainen, J., Roychoudhury, S., Rathi, B., Kumar, D., 2021. Oxidative stress in cancer cell metabolism. Antioxidants 10 (5), 642. https://doi.org/10.3390/antiox10050642.

Arroyo-Acevedo, J., Chávez-Asmat, R.J., Anampa-Guzmán, A., Donaires, R., Ráez-Gonzáles, J., 2015. Protective effect of piper aduncum capsule on DMBA-induced breast cancer in rats. Breast Cancer : Basic Clin. Res. 9, 41–48. https://doi.org/10.4137/BCBCR.S24420.

Aval, M.B., Mehri, E.H., Mombeiny, R., Kazemi, M., Saeedi, S., Tavakol, S., 2023. Dutasteride nanoemulsion preparation to inhibit 5-alpha-hair follicle reductase enzymes in the hair follicle; an ex vivo study. IET Nanobiotechnol. 17 (1), 13–21. https://doi.org/10.1049/nbt2.12101.

Barras, B.J., Ling, T., Rivas, F., 2024. Recent advances in chemistry and antioxidant/anticancer biology of monoterpene and meroterpenoid natural product. Molecules 29 (1), 279. https://doi.org/10.3390/molecules29010279.

Bezerra, D.P., Castro, F.O., Alves, A.P.N.N., Pessoa, C., Moraes, M.O., Silveira, E.R., Lima, M.a.S., Elmiro, F.J.M., Costa-Lotufo, L.V., 2006. In Vivo growth-inhibition of sarcoma 180 by piplartine and piperine, two alkaloid amides from piper. Braz. J. Med. Biol. Res. 39, 801–807. https://doi.org/10.1590/S0100-879X2006000600014.

Bhattacharjee, S., 2016. DLS and zeta potential – what they are and what they are not? J. Control. Release 235, 337–351. https://doi.org/10.1016/j.jconrel.2016.06.017.

Bhattacharya, S., 2020. Fabrication and characterization of chitosan-based polymeric nanoparticles of imatinib for colorectal cancer targeting application. Int. J. Biol. Macromol. 151, 104–115. https://doi.org/10.1016/j.ijbiomac.2020.02.151.

Boisseau, P., Loubaton, B., 2011. Nanomedicine, nanotechnology in medicine. C. R. Phys. 12 (7), 620–636. https://doi.org/10.1016/j.crhy.2011.06.001.

Booth, J.K., Bohlmann, J., 2019. Terpenes in cannabis sativa – from plant genome to humans. Plant Sci. 284, 67–72. https://doi.org/10.1016/j.plantsci.2019.03.022.

Boyles, F., Deane, C.M., Morris, G.M., 2020. Learning from the ligand: using ligand-based features to improve binding affinity prediction. Bioinformatics 36 (3), 758–764. https://doi.org/10.1093/bioinformatics/btz665.

Brigger, I., Dubernet, C., Couvreur, P., 2012. Nanoparticles in cancer therapy and diagnosis. Adv. Drug Deliv. Rev. 64, 24–36. https://doi.org/10.1016/j.addr.2012.09.006.

Conde-Hernández, L.A., Espinosa-Victoria, J.R., Trejo, A., Guerrero-Beltrán, J.Á., 2017. CO2-supercritical extraction, hydrodistillation and steam distillation of essential oil of rosemary (Rosmarinus Officinalis). J. Food Eng. 200, 81–86. https://doi.org/10.1016/j.jfoodeng.2016.12.022.

da Silva, S., Alan, W., Vranken, W.F., 2012. ACPYPE - AnteChamber PYthon parser interface. BMC. Res. Notes 5 (1), 367. https://doi.org/10.1186/1756-0500-5-367.

da Silva, Aristeu Vieira, and Helio Langoni. 2001. "The Detection of Toxoplasma Gondii by Comparing Cytology, Histopathology, Bioassay in Mice, and the Polymerase Chain Reaction (PCR)." Veterin. Parasitol. 97(3): 193–200. doi:10.1016/S0304-4017(01)00404-6.

Daina, A., Michielin, O., Zoete, V., 2017. SwissADME: a free web tool to evaluate pharmacokinetics, drug-likeness and medicinal chemistry friendliness of small molecules. Sci. Rep. 7 (1), 42717. https://doi.org/10.1038/srep42717.

Duda, W., Curzytek, K., Kubera, M., Iciek, M., Kowalczyk-Pachel, D., Bilska-Wilkosz, A., Lorenc-Koci, E., et al., 2016. The effect of chronic mild stress and imipramine on the markers of oxidative stress and antioxidant system in rat liver. Neurotox. Res. 30, 173. https://doi.org/10.1007/s12640-016-9614-8.

Duran, T., Minatovicz, B., Bai, J., Shin, D., Mohammadiarani, H., Chaudhuri, B., 2021. Molecular dynamics simulation to uncover the mechanisms of protein instability during freezing. J. Pharm. Sci. 110 (6), 2457–2471. https://doi.org/10.1016/j.xphs.2021.01.002.

Efdi, M., Fujita, S., Inuzuka, T., Koketsu, M., 2010. Chemical Studies on Goniothalamus Tapis Miq. Nat. Prod. Res. 24 (7), 657–662. https://doi.org/10.1080/14786410903132449.

Eltayeb, N., Ng, S., Ismail, Z., Salhimi, S., 2016. Anti-invasive effect of catharanthus roseus extract on highly metastatic human breast cancer MDA-MB-231 cells. Jurnal Teknologi 78. https://doi.org/10.11113/jt.v78.9870.

Emtiazi, H., Sharif, A.S., Hemati, M., Haghiralsadat, B.F., Pardakhti, A., 2022. Comparative study of nano-liposome and nano-niosome for delivery of achillea millefolium essential oils: development, optimization, characterization and their cytotoxicity effects on cancer cell lines and antibacterial activity. Chem. Biodivers. 19 (10), e202200397.

Fernando, M.D., Maduranganie, A.A., Senathilake, N.H.K.S., Dilip, E., de Silva, C., Nanayakkara, M., Wijesundera, R.L.C., Soysa, P., Kolitha de Silva, B.G.D.N., 2019. In silico pharmacological analysis of a potent anti-hepatoma compound of mushroom origin and emerging role as an adjuvant drug lead. Food Nutr. Sci. 10 (11), 1313–1333. https://doi.org/10.4236/fns.2019.1011095.

Furuhashi, T., Okuda, K., 2017. Application of GC/MS soft ionization for isomeric biological compound analysis. Crit. Rev. Anal. Chem. 47 (5), 438–453. https://doi.org/10.1080/10408347.2017.1320215.

Ganesan, K., Wang, Y., Gao, F., Liu, Q., Zhang, C., Li, P., Zhang, J., Chen, J., 2021. Targeting engineered nanoparticles for breast cancer therapy. Pharmaceutics 13 (11), 1829. https://doi.org/10.3390/pharmaceutics13111829.

Gavas, S., Quazi, S., Karpiński, T.M., 2021. Nanoparticles for cancer therapy: current progress and challenges. Nanoscale Res. Lett. 16, 173. https://doi.org/10.1186/s11671-021-03628-6.

Giunti, G., Palermo, D., Laudani, F., Algeri, G.M., Campolo, O., Palmeri, V., 2019. Repellence and acute toxicity of a nano-emulsion of sweet orange essential oil toward two major stored grain insect pests. Ind. Crop. Prod. 142, 111869 https://doi.org/10.1016/j.indcrop.2019.111869.

Gleeson, M.P., Hersey, A., Montanari, D., Overington, J., 2011. Probing the links between in vitro potency, ADMET and physicochemical parameters. Nat. Rev. Drug Discov. 10 (3), 197–208. https://doi.org/10.1038/nrd3367.

Greay, S.J., Hammer, K.A., 2015. Recent developments in the bioactivity of mono- and diterpenes: anticancer and antimicrobial activity. Phytochem. Rev. 14 (1), 1–6. https://doi.org/10.1007/s11101-011-9212-6.

Gurunathan, S., Han, J.W., Eppakayala, V., Jeyaraj, M., Kim, J.-H., 2013. Cytotoxicity of biologically synthesized silver nanoparticles in MDA-MB-231 human breast cancer cells. Biomed Res. Int. 2013, e535796.

Gyurászová, M., Kovalčíková, A., Janšáková, K., Šebeková, K., Celec, P., Tóthová, Ľ., 2018. Markers of oxidative stress and antioxidant status in the plasma, urine and saliva of healthy mice. Physiol. Res. 921–34 https://doi.org/10.33549/physiolres.933866.

Hadwan, M.H., 2018. Simple spectrophotometric assay for measuring catalase activity in biological tissues. BMC Biochem. 19 (1), 7. https://doi.org/10.1186/s12858-018-0097-5.

Heidari, F., Rabizadeh, S., Mansournia, M.A., Mirmiranpoor, H., Salehi, S.S., Akhavan, S., Esteghamati, A., Nakhjavani, M., 2019. Inflammatory, oxidative stress and anti-oxidative markers in patients with endometrial carcinoma and diabetes. Cytokine 120, 186–190. https://doi.org/10.1016/j.cyto.2019.05.007.

Hsu, H.-Y., Chen, B.-H., 2022. A comparative study on inhibition of breast cancer cells and tumors in mice by carotenoid extract and nanoemulsion prepared from sweet potato (ipomoea batatas l.) peel. Pharmaceutics 14 (5), 980. https://doi.org/10.3390/pharmaceutics14050980.

Hussain, A., Bourguet-Kondracki, M.-L., Hussain, F., Rauf, A., Ibrahim, M., Khalid, M., Hussain, H., et al., 2022. The potential role of dietary plant ingredients against mammary cancer: a comprehensive review. Crit. Rev. Food Sci. Nutr. 62 (10), 2580–2605. https://doi.org/10.1080/10408398.2020.1855413.

Il'ina, Irina V., Nadezhda S. Dyrkheeva, Alexandra L. Zakharenko, Alexander Yu Sidorenko, Nikolay S. Li-Zhulanov, Dina V. Korchagina, Raina Chand, et al. 2020. "Design, Synthesis, and Biological Investigation of Novel Classes of 3-Carene-Derived Potent Inhibitors of TDP1." *Molecules* 25(15): 3496. doi:10.3390/molecules25153496.

Jang, S.S., Kim, H.G., Lee, J.S., Han, J.M., Park, H.J., Huh, G.J., Son, C.G., 2013. Melatonin reduces X-Ray radiation-induced lung injury in mice by modulating oxidative stress and cytokine expression. Int. J. Radiat Biol. 89 (2), 97–105. https://doi.org/10.3109/09553002.2013.734943.

Johnson, R., Sabnis, N., McConathy, W.J., Lacko, A.G., 2013. The potential role of nanotechnology in therapeutic approaches for triple negative breast cancer. Pharmaceutics 5 (2), 353–370. https://doi.org/10.3390/pharmaceutics5020353.

Kaplan, H.G., Malmgren, J.A., Atwood, M.K., 2017. Triple-negative breast cancer in the elderly: prognosis and treatment. Breast J. 23 (6), 630–667. https://doi.org/10.1111/tbj.12813.

Kim, J., Woo, H.K., Vimalajeewa, D., Vidakovic, B., 2023. Analysis and classification of 1H-NMR spectra by multifractal analysis. PLoS One 18 (6), e0286205.

Kumar, S., Singh, B., Singh, R., 2022. Catharanthus roseus (L.) G. Don: a review of its ethnobotany, phytochemistry, ethnopharmacology and toxicities. J. Ethnopharmacol. 284, 114647 https://doi.org/10.1016/j.jep.2021.114647.

Kuttan, G., Pratheeshkumar, P., Manu, K.A., Kuttan, R., 2011. Inhibition of tumor progression by naturally occurring terpenoids. Pharm. Biol. 49 (10), 995–1007. https://doi.org/10.3109/13880209.2011.559476.

Lawal, O.A., Ogunwande, I.A., Ibirogba, A.E., Layode, O.M., Opoku, A.R., 2015. Chemical constituents of essential oils from catharanthus roseus (L.) G. Don Grown in Nigeria. J. Essential Oil Bearing Plants 18 (1), 57–63. https://doi.org/10.1080/0972060X.2014.998720.

Lindemann, R. K., A. Newbold, K. F. Whitecross, L. A. Cluse, A. J. Frew, L. Ellis, S. Williams, et al. 2007. "Analysis of the Apoptotic and Therapeutic Activities of Histone Deacetylase Inhibitors by Using a Mouse Model of B Cell Lymphoma." *Proceedings of the National Academy of Sciences* 104(19): 8071–76. doi:10.1073/pnas.0702294104.

Liyanage, P.Y., Hettiarachchi, S.D., Zhou, Y., Ouhtit, A., Seven, E.S., Oztan, C.Y., Celik, E., Leblanc, R.M., 2019. "Nanoparticle-mediated targeted drug delivery for

breast cancer treatment". Biochim. et Biophys. Acta (BBA) – Rev. Cancer 1871 (2), 419–433. https://doi.org/10.1016/j.bbcan.2019.04.006.
Luis, C., Castaño-Guerrero, Y., Soares, R., Sales, G., Fernandes, R., 2019. Avoiding the interference of doxorubicin with MTT measurements on the MCF-7 breast cancer cell line. Methods and Protocols 2 (2), 29. https://doi.org/10.3390/mps2020029.
Madka, V., Rao, C.V., 2013. Anti-inflammatory phytochemicals for chemoprevention of colon cancer. Curr. Cancer Drug Targets 13 (5), 542–557.
Malik, Z., Parveen, R., Abass, S., Dar, M.I., Husain, S.A., Ahmad, S., 2022. Receptor-mediated targeting in breast cancer through solid lipid nanoparticles and its mechanism. Curr. Drug Metab. 23 (10), 800–817. https://doi.org/10.2174/1389200223666220416213639.
Maqbool, T., Awan, S.J., Malik, S., Hadi, F., Shehzadi, S., Tariq, K., 2019. In-vitro anti-proliferative, apoptotic and antioxidative activities of medicinal herb kalonji (nigella sativa). Curr. Pharm. Biotechnol. 20 (15), 1288–1308. https://doi.org/10.2174/1389201020666190821144633.
Marefati, N., Beheshti, F., Vafaee, F., Barabadi, M., Hosseini, M., 2021. The effects of incensole acetate on neuro-inflammation, brain-derived neurotrophic factor and memory impairment induced by lipopolysaccharide in rats. Neurochem. Res. 46 (9), 2473–2484. https://doi.org/10.1007/s11064-021-03381-3.
Moussaieff, Arieh, Na'ama A Shein, Jeanna Tsenter, Savvas Grigoriadis, Constantina Simeonidou, Alexander G Alexandrovich, Victoria Trembovler, et al. 2008. "Incensole Acetate: A Novel Neuroprotective Agent Isolated from Boswellia Carterii." J. Cereb. Blood Flow Metab. 28(7): 1341–52. doi:10.1038/jcbfm.2008.28.
Ngo, Y.L., Chua, L.S., 2019. Column chromatography for preparing rosmarinic acid rich extract from orthosiphon aristatus. J. Liq. Chromatogr. Relat. Technol. 42 (17–18), 546–554. https://doi.org/10.1080/10826076.2019.1635891.
Ombredane, A.S., Araujo, V.H.S., Borges, C.O., Costa, P.L., Landim, M.G., Pinheiro, A.C., Szlachetka, Í.O., et al., 2020. Nanoemulsion-based systems as a promising approach for enhancing the antitumoral activity of pequi oil (caryocar brasilense cambess.) in breast cancer cells. J. Drug Delivery Sci. Technol. 58, 101819 https://doi.org/10.1016/j.jddst.2020.101819.
Ourzeddine, W., D'Ambola, M., Malafronte, N., León, F., Brouard, I., Benayache, F., Benayache, S., 2017. A new Δ-2-Carene-β-D-glucopyranoside from fagonia longispina. Nat. Prod. Commun. 12 (9) https://doi.org/10.1177/1934578X1701200901, 1934578X1701200901.
Parthasarathy, M., Prince, S.E., 2021. The potential effect of phytochemicals and herbal plant remedies for treating drug-induced hepatotoxicity: a review. Mol. Biol. Rep. 48 (5), 4767–4788. https://doi.org/10.1007/s11033-021-06444-4.
Periasamy, V.S., Athinarayanan, J., Alshatwi, A.A., 2016. Anticancer activity of an ultrasonic nanoemulsion formulation of nigella sativa L. essential oil on human breast cancer cells. Ultrason. Sonochem. 31, 449–455. https://doi.org/10.1016/j.ultsonch.2016.01.035.
Pham, Hong Ngoc Thuy, Jennette A. Sakoff, Quan Van Vuong, Michael C. Bowyer, and Christopher J. Scarlett. 2019. "Phytochemical, antioxidant, anti-proliferative and antimicrobial properties of catharanthus roseus root extract, saponin-enriched and aqueous fractions." Mol. Biol. Rep. 46(3): 3265–73. doi:10.1007/s11033-019-04786-8.
Rahmani, F., Nabi, S., Idliki, R., Alimirzaei, M., Barkhordar, S.M.A., Shafaei, N., Zareian, M., Karimi, E., Oskoueian, E., 2022. Thyme oil nanoemulsion enhanced cellular antioxidant and suppressed inflammation in mice challenged by cadmium-induced oxidative stress. Waste Biomass Valoriz. 13, 1–8. https://doi.org/10.1007/s12649-022-01738-5.
Rajivgandhi, G., Saravanan, K., Ramachandran, G., Li, J.-L., Yin, L., Quero, F., Alharbi, N. S., et al., 2020. Enhanced anti-cancer activity of chitosan loaded morinda citrifolia essential oil against A549 human lung cancer cells. Int. J. Biol. Macromol. 164, 4010–4021. https://doi.org/10.1016/j.ijbiomac.2020.08.169.
Ren, Z., Liang, H., Galbo, P.M., Dharmaratne, M., Kulkarni, A.S., Fard, A.T., Aoun, M.L., et al., 2022. Redox signaling by glutathione peroxidase 2 links vascular modulation to metabolic plasticity of breast cancer. Proc. Natl. Acad. Sci. 119 (8) https://doi.org/10.1073/pnas.2107266119 e2107266119.
Rohman, A., Wijayanti, T., Windarsih, A., Riyanto, S., 2020. The authentication of java turmeric (Curcuma Xanthorrhiza) using thin layer chromatography and 1H-NMR based-metabolite fingerprinting coupled with multivariate analysis. Molecules 25 (17), 3928. https://doi.org/10.3390/molecules25173928.
Rojas-Armas, J.P., Arroyo-Acevedo, J.L., Palomino-Pacheco, M., Ortiz-Sánchez, J.M., Calva, J., Justil-Guerrero, H.J., Castro-Luna, A., et al., 2022. Phytochemical constituents and ameliorative effect of the essential oil from annona muricata l. leaves in a murine model of breast cancer. Molecules 27 (6), 1818. https://doi.org/10.3390/molecules27061818.
Samec, M., Liskova, A., Koklesova, L., Samuel, S.M., Murin, R., Zubor, P., Bujnak, J., et al., 2020. The role of plant-derived natural substances as immunomodulatory agents in carcinogenesis. J. Cancer Res. Clin. Oncol. 146 (12), 3137–3154. https://doi.org/10.1007/s00432-020-03424-2.
Shaldam, M., Nocentini, A., Elsayed, Z.M., Ibrahim, T.M., Salem, R., El-Domany, R.A., Capasso, C., Supuran, C.T., Eldehna, W.M., 2021. Development of novel quinoline-based sulfonamides as selective cancer-associated carbonic anhydrase isoform IX inhibitors. Int. J. Mol. Sci. 22 (20), 11119. https://doi.org/10.3390/ijms222011119.
Sharma, T., Suresh Kumar, G., Chon, B.H., Sangwai, J.S., 2014. Viscosity of the oil-in-water pickering emulsion stabilized by surfactant-polymer and nanoparticle-surfactant-polymer system. Korea-Australia Rheol. J. 26 (4), 377–387. https://doi.org/10.1007/s13367-014-0043-z.
Shoorvarzi, N., Somayeh, F.S., Shafaei, N., Karimi, E., Oskoueian, E., 2020. Citrus aurantium l. bloom essential oil nanoemulsion: synthesis, characterization, cytotoxicity, and its potential health impacts on mice. J. Food Biochem. 44 (5), e13181.
Shu, H., Chen, H., Wang, X., Yueying, Hu., Yun, Y., Zhong, Q., Chen, W., Chen, W., 2019. Antimicrobial activity and proposed action mechanism of 3-carene against brochothrix thermosphacta and pseudomonas fluorescens. Molecules 24 (18), 3246. https://doi.org/10.3390/molecules24183246.
Singh, V.K., Arora, D., Ansari, M.I., Sharma, P.K., 2019. Phytochemicals based chemopreventive and chemotherapeutic strategies and modern technologies to overcome limitations for better clinical applications. Phytother. Res. 33 (12), 3064–3089. https://doi.org/10.1002/ptr.6508.
Spyridopoulou, K., Fitsiou, E., Bouloukosta, E., Tiptiri-Kourpeti, A., Vamvakias, M., Oreopoulou, A., Papavassilopoulou, E., Pappa, A., Chlichlia, K., 2019. Extraction, chemical composition, and anticancer potential of origanum onites l. essential oil. Molecules 24 (14), 2612. https://doi.org/10.3390/molecules24142612.
Srivastava, A.K., Bhatnagar, P., Singh, M., Mishra, S., Kumar, P., Shukla, Y., Gupta, K.C., 2013. Synthesis of PLGA nanoparticles of tea polyphenols and their strong in vivo protective effect against chemically induced DNA damage. Int. J. Nanomed. 8, 1451–1462. https://doi.org/10.2147/IJN.S26364.
Talkington, A., Durrett, R., 2015. Estimating tumor growth rates in vivo. Bull. Math. Biol. 77 (10), 1934–1954. https://doi.org/10.1007/s11538-015-0110-8.
Thoppil, R.J., 2011. Terpenoids as potential chemopreventive and therapeutic agents in liver cancer. World J. Hepatol. 3 (9), 228. https://doi.org/10.4254/wjh.v3.i9.228.
Thulasidas, J., Sadasivam, P., Varadarajan, G., 2019. "Cancer-fighting phytochemicals. Another Look". 9, 162. https://doi.org/10.4172/2155-983X.1000162.
Tomko, A.M., Whynot, E.G., Ellis, L.D., Dupré, D.J., 2020. Anti-Cancer potential of cannabinoids, terpenes, and flavonoids present in cannabis. Cancers 12 (7), 1985. https://doi.org/10.3390/cancers12071985.
Tubtimsri, S., Limmatvapirat, C., Limsirichaikul, S., Akkaramongkolporn, P., Piriyaprasarth, S., Patomchaiviwat, V., Limmatvapirat, S., 2021. Incorporation of fixed oils into spearmint oil-loaded nanoemulsions and their influence on characteristic and cytotoxic properties against human oral cancer cells. J. Drug Delivery Sci. Technol. 63, 102443 https://doi.org/10.1016/j.jddst.2021.102443.
Tüzün, B.S., Hohmann, J., Kivcak, B., 2018. Green bio-inspired synthesis, characterization and activity of silver nanoparticle forms of centaurea virgata lam. and the isolated flavonoid eupatorin. Green Process. Synth, 7 (4), 372–379. https://doi.org/10.1515/gps-2017-0027.
Uncu, O., Ozen, B., Tokatli, F., 2019. Use of FTIR and UV–visible spectroscopy in determination of chemical characteristics of olive oils. Talanta 201, 65–73. https://doi.org/10.1016/j.talanta.2019.03.116.
Valko, M., Leibfritz, D., Moncol, J., Cronin, M.T.D., Mazur, M., Telser, J., 2007. Free radicals and antioxidants in normal physiological functions and human disease. Int. J. Biochem. Cell Biol. 39 (1), 44–84. https://doi.org/10.1016/j.biocel.2006.07.001.
Verma, M., Fatima, S., Ansari, I.A., 2022. Phytofabricated nanoparticle formulation for cancer treatment: a comprehensive review. Curr. Drug Metab. 23 (10), 818–826. https://doi.org/10.2174/1389200223666220427101427.
Vivo, D.e., Marco, M.M., Bottegoni, G., Cavalli, A., 2016. Role of molecular dynamics and related methods in drug discovery. J. Med. Chem. 59 (9), 4035–4061. https://doi.org/10.1021/acs.jmedchem.5b01684.
Vutukuri, V.R., Das, M.C., Reddy, M., Prabodh, S., Sunethri, P., 2017. Evaluation of acute oral toxicity of ethanol leaves extract of catharanthus roseus in wistar albino rats. J. Clin. Diagn. Res. 11 (3), FF01–FF04. https://doi.org/10.7860/JCDR/2017/24937.9325.
Weydert, C.J., Cullen, J.J., 2010. Measurement of superoxide dismutase, catalase, and glutathione peroxidase in cultured cells and tissue. Nat. Protoc. 5 (1), 51–66. https://doi.org/10.1038/nprot.2009.197.
Xiong, Q., Ming, Xu., Li, J., Liu, Y., Jixiang Zhang, Y.X., Dong, W., 2021. Clinical Sequelae of COVID-19 Survivors in Wuhan, China: A Single-Centre Longitudinal Study. Clin. Microbiol. Infect. 27 (1), 89–95. https://doi.org/10.1016/j.cmi.2020.09.023.
Zhao, Y., Chen, R., Wang, Y., Yang, Y., 2018. α-pinene inhibits human prostate cancer growth in a mouse xenograft model. Chemotherapy 63 (1), 1–7. https://doi.org/10.1159/000479863.